

Needle-Tissue Interaction Force Estimation using Residuals and Interaction Models

Medical Robotics Project Report

Roggiani Gianmarco*, Roscia Francesco†, Sodano Matteo†

In the last years, imaging technologies have become a reliable support to the minimally-invasive surgery for different kinds of organ diseases. The classic approach to this interventional procedure is based on free-hand percutaneous placement of needles and probes under image guidance, either with ultrasound (US), computed tomography (CT), fluoroscopy (XA) or magnetic resonance (MR). US and XA offer real-time guidance but cannot visualize deep organs and soft tissues, while CT and MR do not support real-time image acquisition. Moreover, they expose the patient to ionizing radiations. The free-hand approach is subject to inappropriate planning, operator fatigue, patients' movements, etc. A teleoperated robot may increase precision and security, reduce the exposure to radiations for both the patient and the surgeon and remove physiological motions. The problem of real-time image acquisition may be overcome by exploiting the insertion mechanics and estimating the needle-tissue interaction forces [2].

In this work, the goal is to reconstruct the contact forces exerted on the needle mounted on the end-effector of a robot manipulator, in a sensorless fashion. This is been achieved considering that contact as a fault in the actuation system, as in [3], [4]. The considered fault detection and isolation techniques are based on generalized momenta, which requires proprioceptive sensors only. Then, a method for identifying rupture events is presented. Using the Recursive Least Squares (RLS) algorithm, the needle-tissue interaction force is estimated and the estimation error is analyzed to extract information about possible layer transitions, as in [5].

Sensorless Reconstruction of Interaction Forces

Consider the Lagrangian model of a robot manipulator interacting with the environment at the contact point $\mathbf{x}_c \in \mathbb{R}^3$

$$\mathbf{B}(\mathbf{q}) \ddot{\mathbf{q}} + \mathbf{C}(\mathbf{q}, \dot{\mathbf{q}}) \dot{\mathbf{q}} + \mathbf{g}(\mathbf{q}) = \boldsymbol{\tau} + \mathbf{J}_c^T(\mathbf{q}) \mathbf{F} = \boldsymbol{\tau}_{tot} \quad (1)$$

where:

*Master of Science in Artificial Intelligence and Robotics

†Master of Science in Control Engineering

- $\mathbf{q}, \dot{\mathbf{q}}, \ddot{\mathbf{q}} \in \mathbb{R}^n$ are the joint positions, velocities and accelerations, respectively;
- n is the dimension of the configuration space;
- $\mathbf{B} \in \mathbb{R}^{n \times n}$ is the inertia matrix;
- $\mathbf{C} \dot{\mathbf{q}} \in \mathbb{R}^n$ is the centrifugal and Coriolis term;
- $\mathbf{g} \in \mathbb{R}^n$ is the gravity term;
- $\boldsymbol{\tau} \in \mathbb{R}^n$ is the control torque;
- $\mathbf{J}_c \in \mathbb{R}^{6 \times n}$ is the geometric Jacobian of the manipulator at the contact point;
- $\mathbf{F} \in \mathbb{R}^6$ is the vector of force and moment exerted by the environment on the tip of the needle, that is unknown;
- $\boldsymbol{\tau}_{tot} \in \mathbb{R}^n$ is the total torque applied to the robot joints.

The nonconservative forces doing work at the manipulator joints have not been modeled.

Residual Method

Denoting with $\boldsymbol{\tau}_c = \mathbf{J}_c^T(\mathbf{q}) \mathbf{F}$ the joint torque caused by the contact, the generalized momentum $\mathbf{p} = \mathbf{B}(\mathbf{q}) \dot{\mathbf{q}}$ associated to (1) satisfies the first-order equation:

$$\dot{\mathbf{p}} = \boldsymbol{\tau} + \boldsymbol{\tau}_c + \mathbf{C}^T(\mathbf{q}, \dot{\mathbf{q}}) \dot{\mathbf{q}} - \mathbf{g}(\mathbf{q}).$$

Notice that its dynamics is decoupled: the i -th component of $\dot{\mathbf{p}}$ depends only on the i -th component of $\boldsymbol{\tau}_c$, with $i = 1, 2, \dots, n$.

Define the six-dimensional *residual vector* as

$$\mathbf{r}(t) = \mathbf{K} \left[\mathbf{p}(t) - \int_0^t (\boldsymbol{\tau} + \mathbf{C}^T(\mathbf{q}, \dot{\mathbf{q}}) \dot{\mathbf{q}} - \mathbf{g}(\mathbf{q}) + \mathbf{r}) ds - \mathbf{p}(0) \right], \quad (2)$$

with the diagonal gain matrix $\mathbf{K} > 0$. In order to implement (2), measures of the current joint positions and velocities have to be available, and the knowledge of the current commanded torques is required. The dynamics of the residual vector is

$$\dot{\mathbf{r}} = -\mathbf{K} \mathbf{r} + \mathbf{K} \boldsymbol{\tau}_c, \quad \mathbf{r}(0) = 0,$$

i.e., the one of a linear exponentially stable system with the joint contact torque $\boldsymbol{\tau}_c$ as input. Every component of the residual vector dynamics is described by a transfer function of the form

$$\frac{r_i(s)}{\tau_{c,i}(s)} = \frac{K_i}{s + K_i}.$$

During free motion, $\mathbf{r} \approx \mathbf{0}$. When a collision occurs, one or more entries of \mathbf{r} vary. For large values of K_i , the evolution of r_i will reproduce the evolution of $\tau_{c,i}$. Therefore, the

reconstruction error $\boldsymbol{\varepsilon} = \boldsymbol{\tau}_c - \mathbf{r}$ will be close to zero. Residuals return to zero when contact is lost. If the residual vector has the first i components different from zero and the others $n - i$ equal to zero, then a collision has occurred at link i . This is known as *isolation property*. In this work, the contact is experienced only at the tip of the needle, causing the whole residual vector to be non-null.

Finally, \mathbf{F} is reconstructed as

$$\hat{\mathbf{F}}_{RES} = [\mathbf{J}_c^T(\mathbf{q})]^\# \mathbf{r}, \quad (3)$$

where $(\cdot)^\#$ denotes the pseudo-inverse operation.

Assuming a perfectly rigid needle, the penetration occurs only along the end-effector z -axis. Thus, we denote with \hat{f}_{RES} the third component of $\hat{\mathbf{F}}_{RES}$.

Discretization of Residual Equation

In order to estimate the force exerted on the needle, equation (2) has to be discretized. The Euler integration method has been used with time step Δt . In the following, we denote with \mathbf{B}_k the inertia matrix at step k (i.e., $\mathbf{B}(\mathbf{q}_k)$), with \mathbf{C}_k the Coriolis and centrifugal term at step k (i.e., $\mathbf{C}(\mathbf{q}_k, \dot{\mathbf{q}}_k)$), with \mathbf{g}_k the gravity term at step k (i.e., $\mathbf{g}(\mathbf{q}_k)$), and with \mathbf{p}_0 the initial value of the generalized momentum (i.e., $\mathbf{p}(0)$). Substituting the generalized momentum formula into (2) and discretizing it, we got:

$$\begin{aligned} \mathbf{r}_k &= \mathbf{K} \left[\mathbf{B}_k \dot{\mathbf{q}}_k - \sum_{i=0}^k (\boldsymbol{\tau}_i + \mathbf{C}_i^T \dot{\mathbf{q}}_i - \mathbf{g}_i + \mathbf{r}_i) \Delta t - \mathbf{p}_0 \right] \\ &= \mathbf{K} \left[\mathbf{B}_k \dot{\mathbf{q}}_k - \sum_{i=0}^k (\boldsymbol{\tau}_i + \mathbf{C}_i^T \dot{\mathbf{q}}_i - \mathbf{g}_i) \Delta t - \left(\sum_{i=0}^{k-1} \mathbf{r}_i + \mathbf{r}_k \right) \Delta t - \mathbf{p}_0 \right]. \end{aligned}$$

Therefore, collecting the residual at the current step, we have obtained:

$$(\mathbf{I}_n + \mathbf{K} \Delta t) \mathbf{r}_k = \mathbf{K} \left[\mathbf{B}_k \dot{\mathbf{q}}_k - \sum_{i=0}^k (\boldsymbol{\tau}_i + \mathbf{C}_i^T \dot{\mathbf{q}}_i - \mathbf{g}_i) \Delta t - \sum_{i=0}^{k-1} \mathbf{r}_i \Delta t - \mathbf{p}_0 \right].$$

Finally, the iterative expression of the residual is derived:

$$\mathbf{r}_k = (\mathbf{I}_n + \mathbf{K} \Delta t)^{-1} \mathbf{K} \left[\mathbf{B}_k \dot{\mathbf{q}}_k - \sum_{i=0}^k (\boldsymbol{\tau}_i + \mathbf{C}_i^T \dot{\mathbf{q}}_i - \mathbf{g}_i) \Delta t - \sum_{i=0}^{k-1} \mathbf{r}_i \Delta t - \mathbf{p}_0 \right], \quad (4)$$

provided with $\mathbf{r}_0 = 0$. The matrix $(\mathbf{I}_n + \mathbf{K} \Delta t)$ is always invertible since $\mathbf{K} > 0$.

Detection of Layer Transitions

The main phases of the needle insertion procedure are introduced. During the contact phase the boundary of the tissue deflects under the action of the needle, which is not

penetrating the tissue yet. The interaction force and the tissue stress increase while the needle displacement decreases. This phase ends when the tissue surface is breached (puncture event). At this stage, the needle penetrates with a sudden drop in the interaction force. The needle is subject to a friction force due to the increasing contact area between the needle shaft and the tissue. A friction force of the same nature, but with opposite sign, acts on the needle shaft during the extraction phase. Figure 1 shows the force acting on the needle tip during an insertion procedure as a function of the displacement.

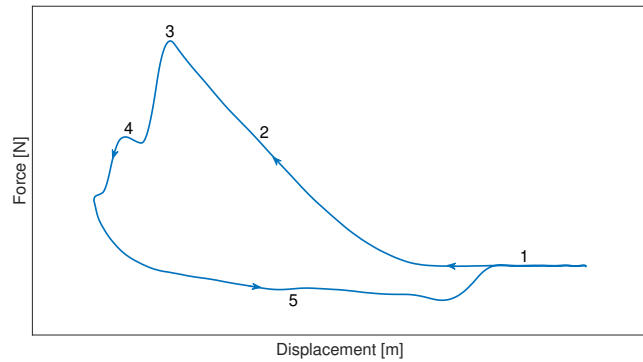


Figure 1: Typical needle-tissue interaction force versus displacement. Five phases can be noticed: no contact (1), contact (2), layer rupture (3), tip and shaft insertion (4), retraction (5)

Interaction Model

Let $p(t)$ be the position of the tip of the needle with respect to the base frame. The interaction forces are described by means of the Kelvin-Voigt generalized model:

$$f(t) = -K(t)p(t) - B(t)\dot{p}(t), \quad (5)$$

where f is the interaction force, K and B are the time-varying elastic and damping coefficients, respectively.

Model (5) captures the elastic force due to the resistance of the layer surface to the needle insertion and the damping force due to the viscous friction along the needle (Figure 2a). The elastic force increases while the needle is pressing on a layer surface and decreases abruptly when the rupture occurs. Equation (5) can be rewritten in matricial form

$$f(t) = \boldsymbol{\varphi}^T(t) \boldsymbol{\theta}(t),$$

denoting with

$$\begin{aligned} \boldsymbol{\varphi}(t) &= \begin{bmatrix} -p(t) & -\dot{p}(t) \end{bmatrix}^T \\ \boldsymbol{\theta}(t) &= \begin{bmatrix} K(t) & B(t) \end{bmatrix}^T. \end{aligned}$$

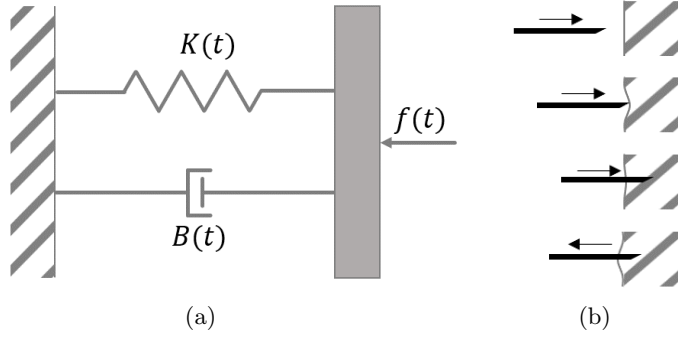


Figure 2: The visco-elastic Kelvin-Voigt model consists of the parallel of a nonlinear spring with a nonlinear damper (left). Needle insertion procedure (right)

Interaction Force Prediction

The RLS algorithm has been used to estimate the interaction force. At step k , the Kelvin-Voigt parameters $\hat{\theta}_k$ and their covariance matrix Ψ_k are estimated as

$$\begin{aligned}\hat{\theta}_k &= \hat{\theta}_{k-1} + \frac{\Psi_{k-1} \varphi_k e_k}{\lambda_k + \varphi_k^T \Psi_{k-1} \varphi_k}, \\ \Psi_k &= \Psi_{k-1} - \frac{\Psi_{k-1} \varphi_k \varphi_k^T \Psi_{k-1}}{\lambda_k + \varphi_k^T \Psi_{k-1} \varphi_k},\end{aligned}\quad (6)$$

where $\lambda_k \in (0, 1]$ is the *forgetting factor* (here, $\lambda_k = 1$, $\forall k$). Denoting with \hat{f}_k the estimated interaction force

$$\hat{f}_k = \varphi_k^T \hat{\theta}_{k-1}, \quad (7)$$

the estimation error is

$$e_k = f_k - \hat{f}_k.$$

In this work, if for a certain step $k^* > 0$ the trace of Ψ_{k^*} falls below a given threshold, then Ψ_{k^*} is replaced with the initial value Ψ_0 . This method is called *Covariance Resetting*, used for having an estimation algorithm more sensitive to parameters variations.

The initial value of the Kelvin-Voigt parameters $\hat{\theta}_0$ is set as

$$\hat{\theta}_0 = [\varphi_0^T]^\# f_0.$$

Layer Transitions

Inspecting the estimation error e_k , transitions between two layers can be detected. As a matter of fact, neglecting modelling errors, disturbances and noise, the estimated force \hat{f}_k should reconstruct well the measured force f_k , unless an abrupt change happens: typically, this is due to a layer rupture.

With $s_k = e_k^2$ as distance function, we introduce the *decision function*

$$g_k = \max\{g_{k-1} + s_k - \nu, 0\}, \quad g_0 = 0. \quad (8)$$

When $g_k > \gamma$, a puncturing event is supposed to occur. The parameters γ (threshold) and ν (drift) are defined as

$$\begin{aligned} \gamma &= \frac{\sigma_1^2 - \sigma_0^2}{2} \\ \nu &= \frac{\sigma_1^2 + \sigma_0^2}{2} \end{aligned}, \quad (9)$$

where σ_0^2 and σ_1^2 are the variances of the error function in the default and abrupt change case, respectively.

We introduce the boolean function

$$\text{Flag}(g_k) = \begin{cases} 1, & \text{if } g_k > \gamma \\ 0, & \text{otherwise} \end{cases},$$

so that a layer transition is supposed to be found when Flag raises.

We present now an off-line method for identifying σ_0 and σ_1 based on a statistical analysis of e_k and its first order time derivative.

1. From the plot of the measured force, identify the number N of expected layer transitions. Notice that each transition introduces a peak in e (therefore, two consecutive peaks in \dot{e}).
2. Compute the local maxima of $|\dot{e}|$ and sort them in decreasing order. Pick the $(2N + 1) - th$ one: because of the above reasoning, it should not depend on any abrupt event, but only on modelling errors, disturbances and noise. Denote the value of this peak with ρ .
3. Divide the time in two disjoint sets, Ω and Ξ . Consider the $i - th$ abrupt event and the related couple of positive and negative consecutive peaks in \dot{e} . Denote with:
 - $t_{\text{IN},i}$ the first time instant for which $\dot{e}(t_{\text{IN},i}) \leq -\rho$;
 - $t_{\text{FIN},i}$ the last time instant for which $\dot{e}(t_{\text{FIN},i}) \geq \rho$.

The elements of Ω are the times for which a puncturing event is expected to occur, while Ξ contains the others:

$$\begin{aligned} \Omega &= \bigcup_i [t_{\text{IN},i}, t_{\text{FIN},i}] \\ \Xi &= \bigcup_i [t_{\text{FIN},i}, t_{\text{IN},i+1}] \end{aligned}. \quad (10)$$

4. Compute σ_0 and σ_1 as

$$\begin{aligned}\sigma_0 &= \text{std}(e(t)), \quad t \in \Xi \\ \sigma_1 &= \text{std}(e(t)), \quad t \in \Omega\end{aligned}, \quad (11)$$

where $\text{std}(\cdot)$ denotes the standard deviation of a sequence of samples.

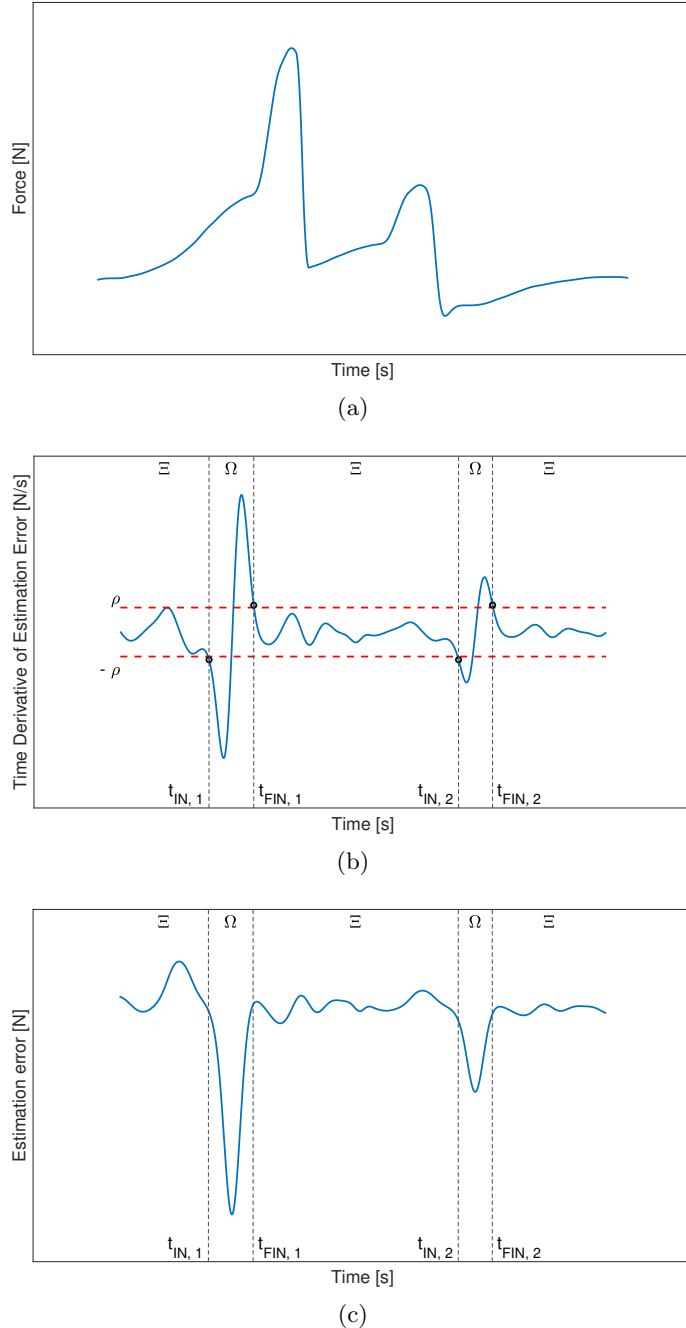


Figure 3: Analyzing the time history of the force along the z -axis, $N = 2$ peaks are found, probably due to layer transitions (a). The threshold ρ is the value of the $(2N + 1) - th$ peak of \dot{e} (b), that is necessary to define Ξ and Ω . These sets are used to compute σ_0 and σ_1 as the variances of e in default and abrupt cases, respectively (c)

We expect that, for different experiments on tissues of the same nature, the values of σ_0 and σ_1 are close enough. Therefore, we believe that the standard deviations can be estimated off-line using the method introduced so far; then, the RLS algorithm for the detection of a puncturing event may run on-line. This conjecture will be investigated computing the values on the available data.

Experimental Setup

The robot manipulator used in this work is the 7R KUKA LWR IV+. The Denavit-Hartenberg frames assignment and parameters are shown in Figure 4.

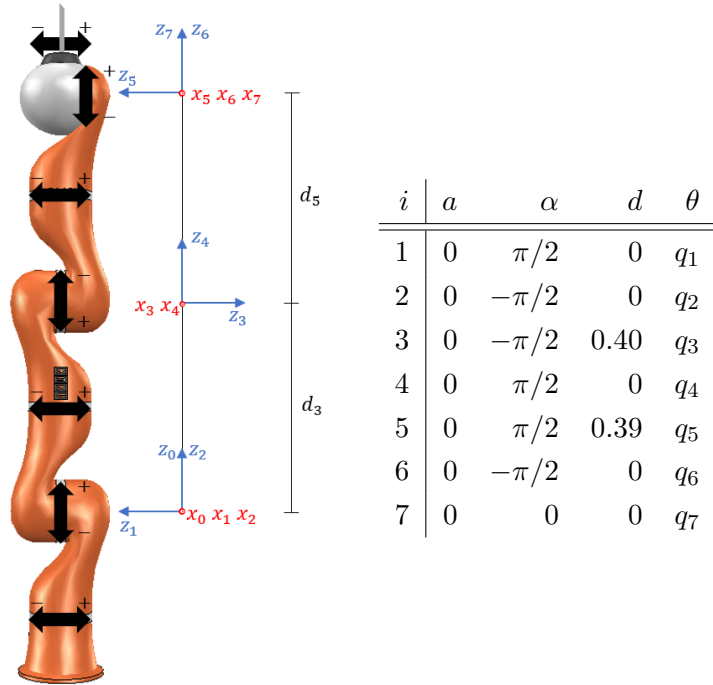


Figure 4: Denavit-Hartenberg frames assignment of the KUKA LWR IV+ robot manipulator (left) and the kinematic parameters (right)

A force/torque sensor is mounted on the robot end-effector together with a needle of length 0.23 m.

Experimental data, retrieved from the Fast Research Interface (FRI) provided by KUKA, have been given to us for the work development. They include:

- joint positions \mathbf{q} ;
- joint torques $\boldsymbol{\tau}_{tot}$;
- external force \mathbf{F} , measured from the force sensor.

These data have been filtered by means of a non-causal Butterworth filter to avoid noise problems. Joint velocities and accelerations have been obtained by numerical differentiation and filtering of $\dot{\mathbf{q}}$. The end-effector position \mathbf{p} and velocity $\dot{\mathbf{p}}$ are obtained using direct and differential kinematics, respectively.

Results

The data provided come from experiments on gel and liver. Gels of different densities are overlapped in order to emulate layers with different mechanic parameters. These simulations are performed both with an sinusoidal automatic trajectory and with a teleoperation system in which the robot is driven by an haptic device, the Geomagic Touch. Two kinds of sinusoidal automatic trajectories are presented, for the gel: in the first one the robot starts in contact with the gel, while in the second one it starts above the gel. Experiments on liver are performed in order to test the algorithm on realistic tissues.

For all the simulations, the residual vector has been computed and compared with the contact torque, computed as $\mathbf{J}_c^T(\mathbf{q}) \mathbf{F}$. The error between these two quantities is also shown. From the residuals, the needle-tissue interaction force has been estimated and compared with the force measured by means of the force/torque sensor. The RLS algorithm has been applied to find the probable occurrences of the layer transitions and to calculate the Kelvin-Voigt parameters. Moreover, we show where and when the rupture events are predicted.

Sinusoidal Automatic Trajectory on Gel - Needle starting in Contact

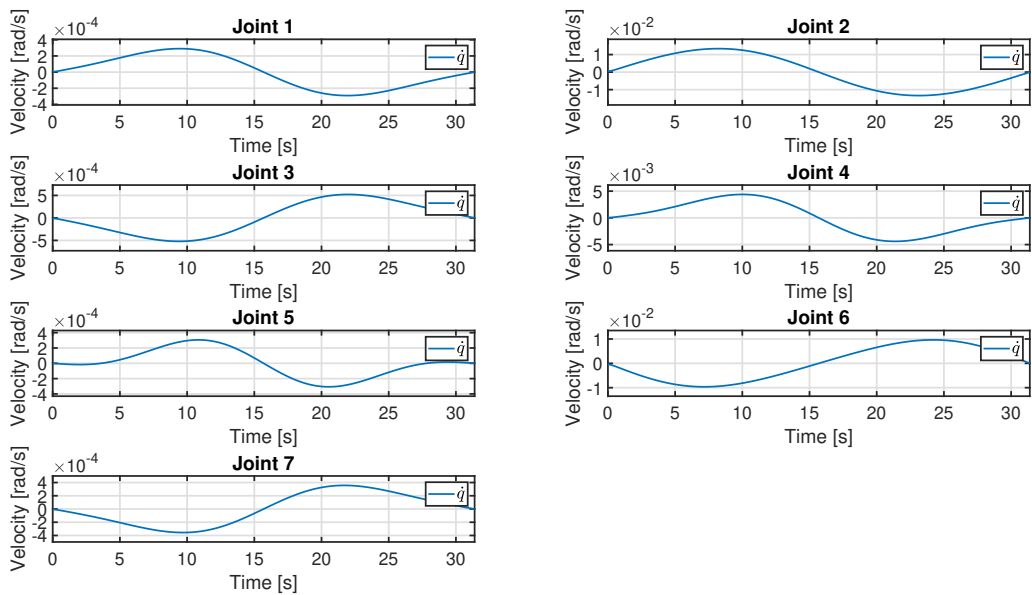


Figure 5: Joint velocities

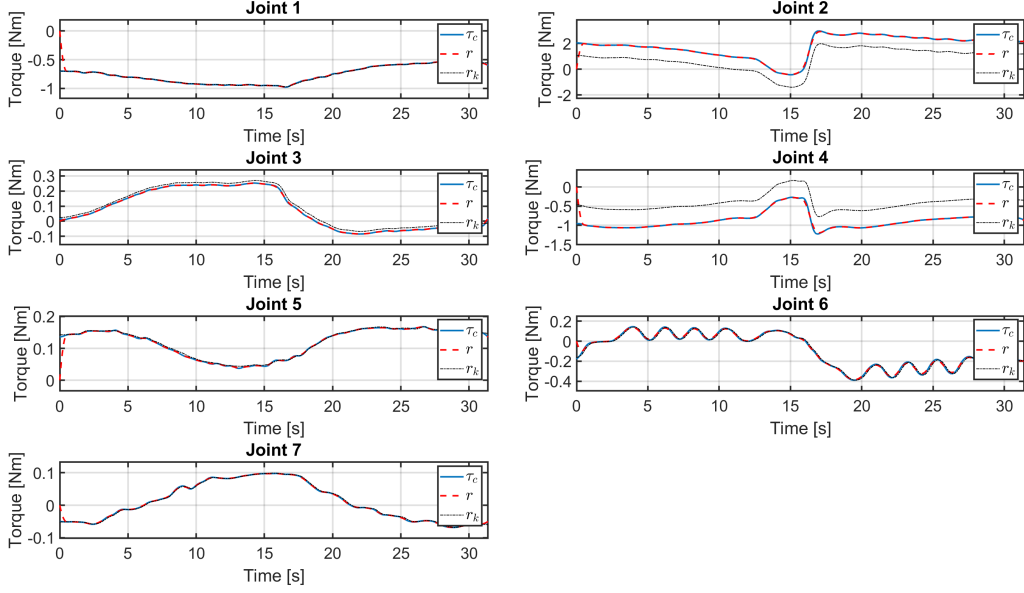


Figure 6: Disturbance joint torque (blue), residuals (red) and residuals retrieved from the Fast Research Interface of KUKA (black)

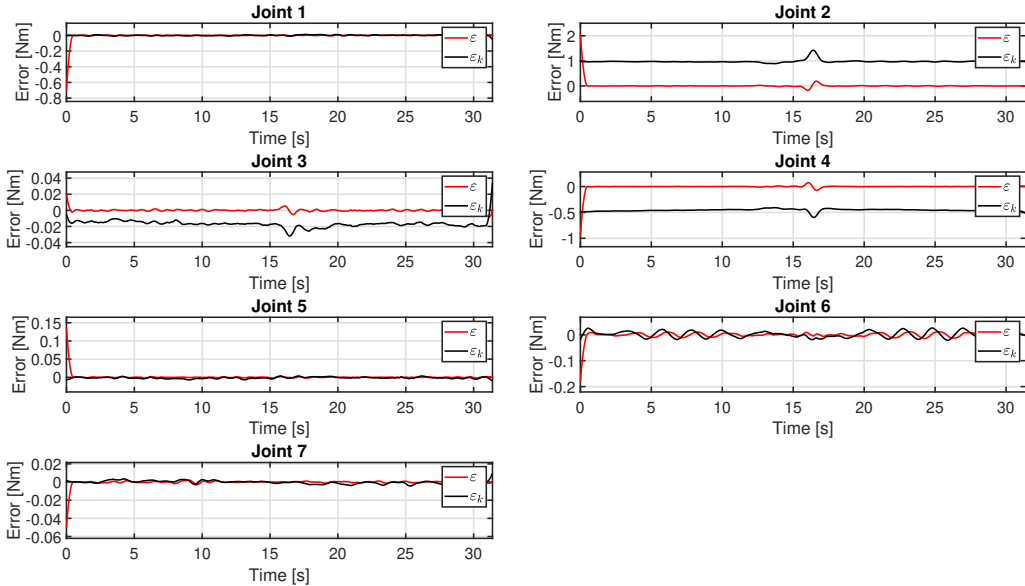


Figure 7: Reconstruction error of residuals (red) and residuals retrieved from the Fast Research Interface of KUKA (black)

The force retrieved from the residual method \hat{f}_{RES} has to be compared with the force obtained from the sensor f : the former is expressed with respect to a frame attached on the needle tip, while the latter is expressed with respect to a frame attached on the last joint of the manipulator (see Figure 4).

This would not make any difference in the case of a completely rigid needle: in fact, a force exerted on the needle tip would not change if translated along the z axis. Since this is not the case, the residual force is computed on the seventh frame for the comparison

with f . The same reasoning is applied for every simulation.

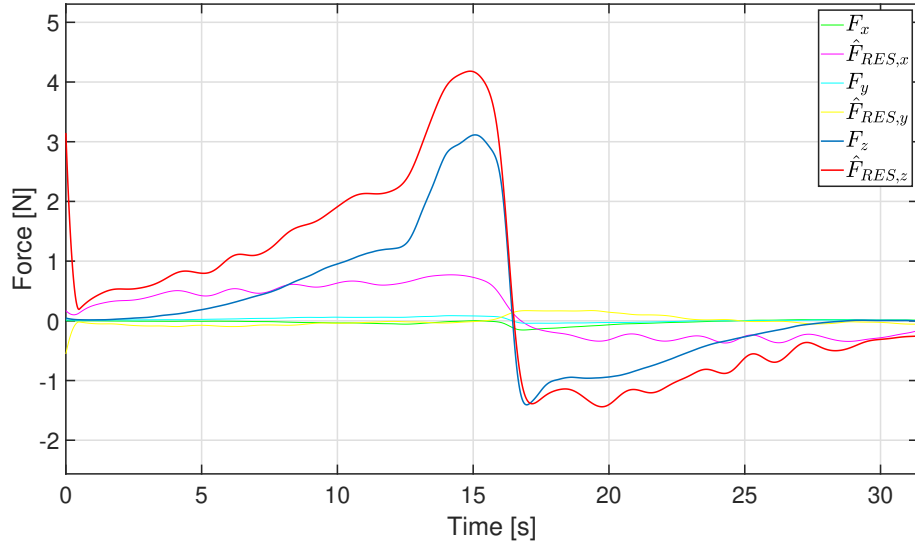


Figure 8: Measured force and reconstructed force from residuals. In particular, the components on the z -axis are in blue (measured) and red (residuals)

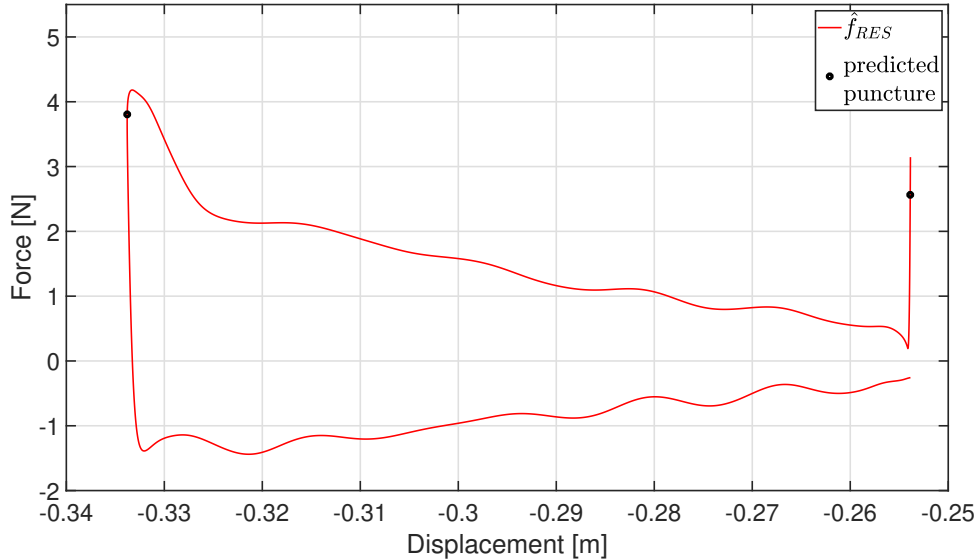


Figure 9: Evolution of the interaction force as a function of displacement. The black points represent the predicted layer transitions

Two layer ruptures are predicted from the algorithm, as seen in Figure 9. Anyway, the second rupture is probably a false positive. In fact, even if the needle is pushing on the underlying layer, the rupture does not occur (notice how the displacement does not increase even if the force decreases). This is caused by the inversion of motion of the needle: in fact, in Figure 11 it can be seen how the flag raises in correspondence with this event.

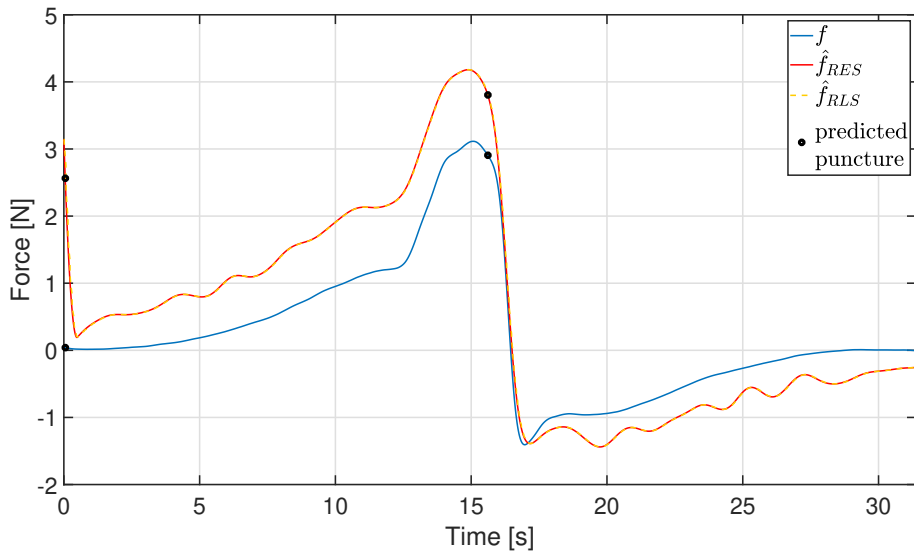
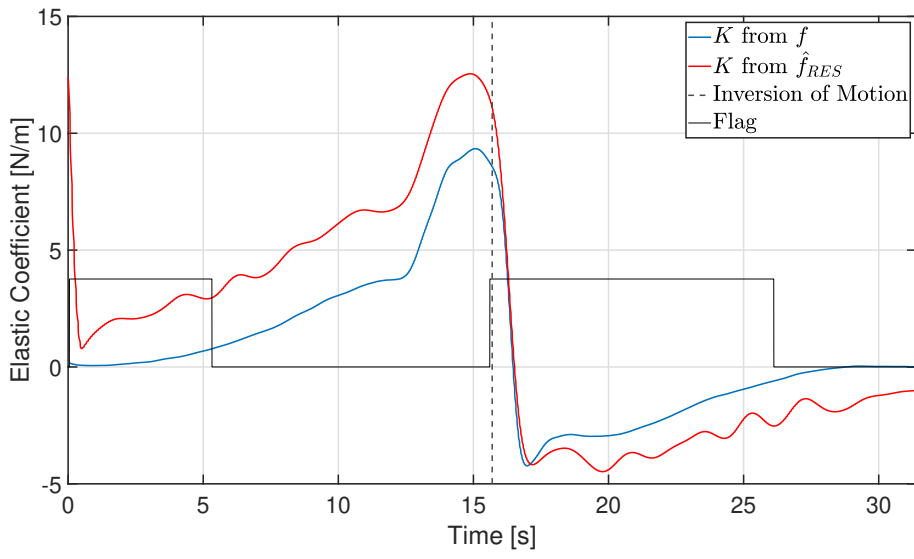


Figure 10: Evolution of the interaction force as a function of time. The black points represent the predicted layer transitions



(a)

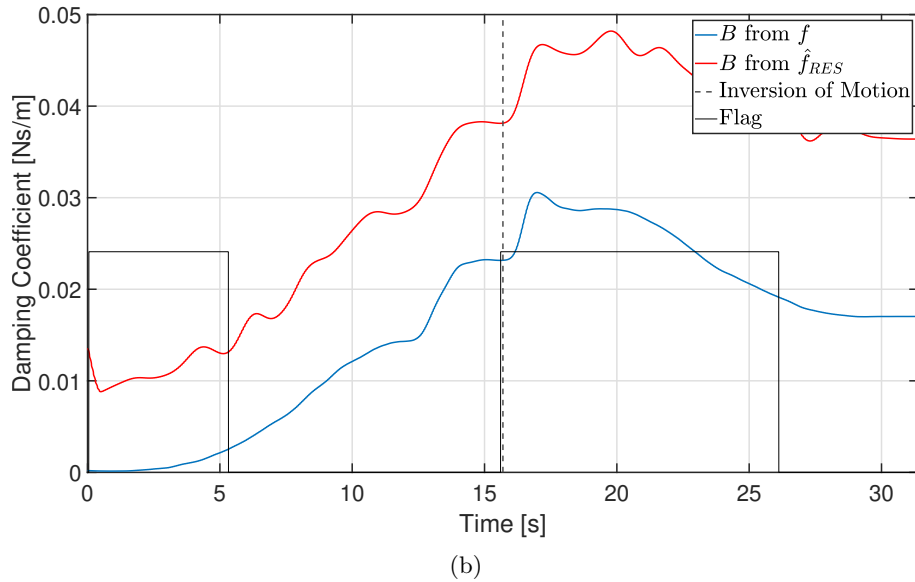


Figure 11: Predicted elastic (a) and damping (b) coefficients, with flag function. In blue, the coefficients obtained from the measured force; in red, the coefficients obtained from the residual force

Data from ten different simulations were available but we reported the results of one sinusoidal automatic trajectory, with the needle starting in contact with the gel. The following plots show the values of σ_0 and σ_1 for all these simulations, together with their average.

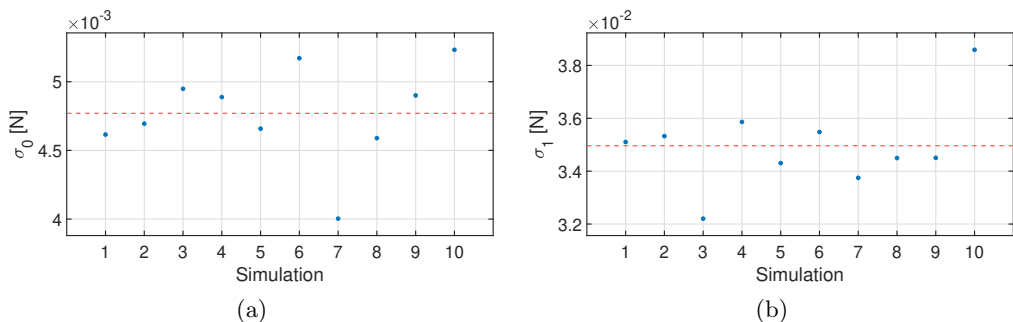


Figure 12: Values of σ_0 (a) and σ_1 (b) for each experiment and their average (red)

Sinusoidal Automatic Trajectory on Gel - Needle starting not in Contact

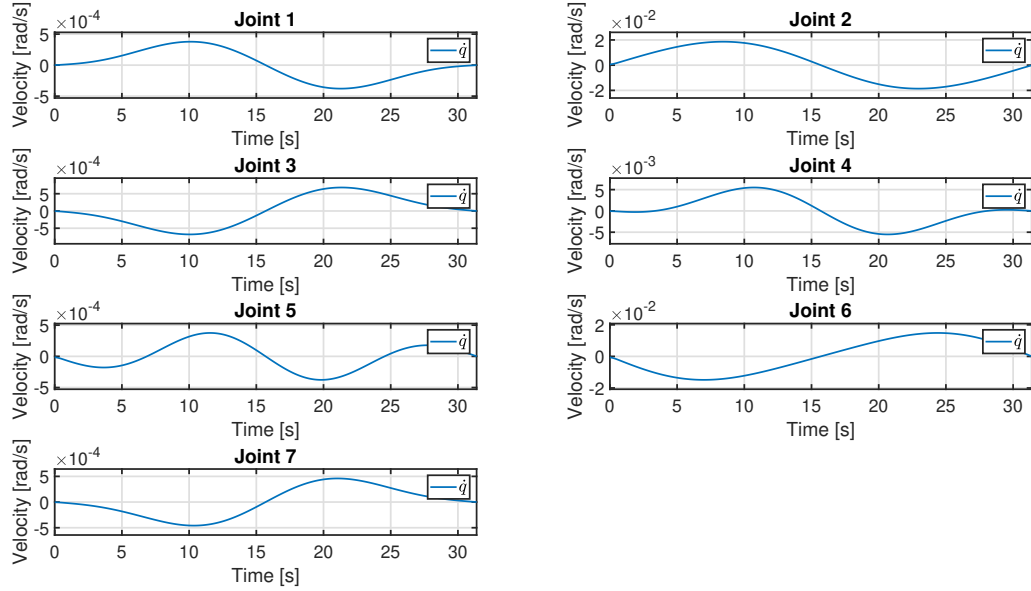


Figure 13: Joint velocities

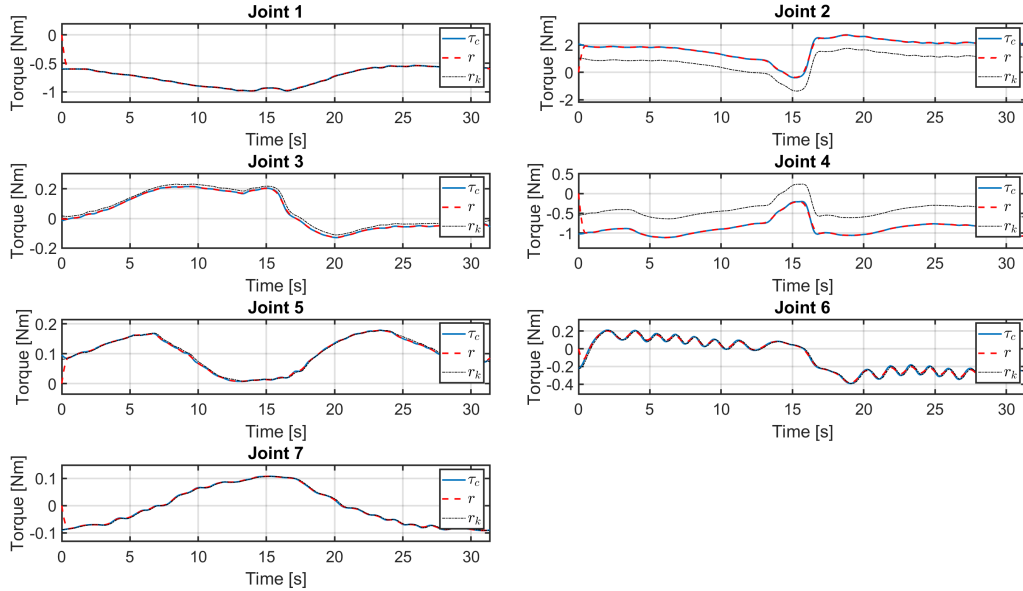


Figure 14: Disturbance joint torque (blue), residuals (red) and residuals retrieved from the Fast Research Interface of KUKA (black)

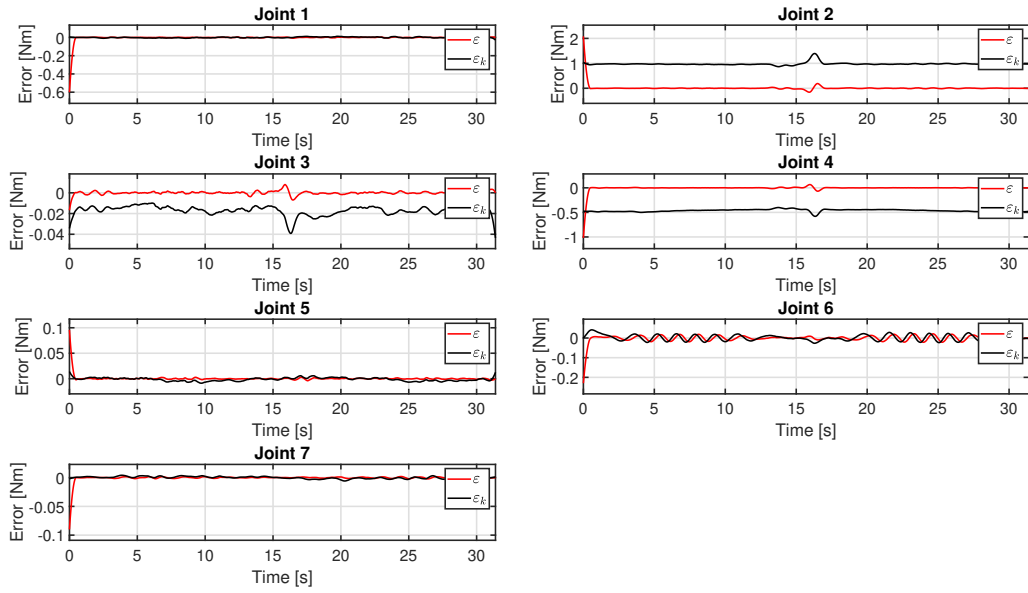


Figure 15: Reconstruction error of residuals (red) and residuals retrieved from the Fast Research Interface of KUKA (black)

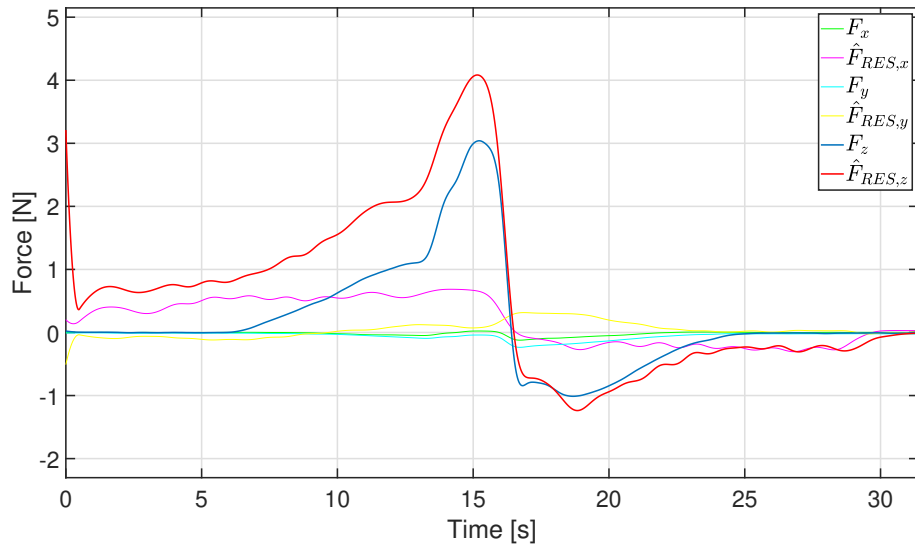


Figure 16: Measured force and reconstructed force from residuals. In particular, the components on the z -axis are in blue (measured) and red (residuals)

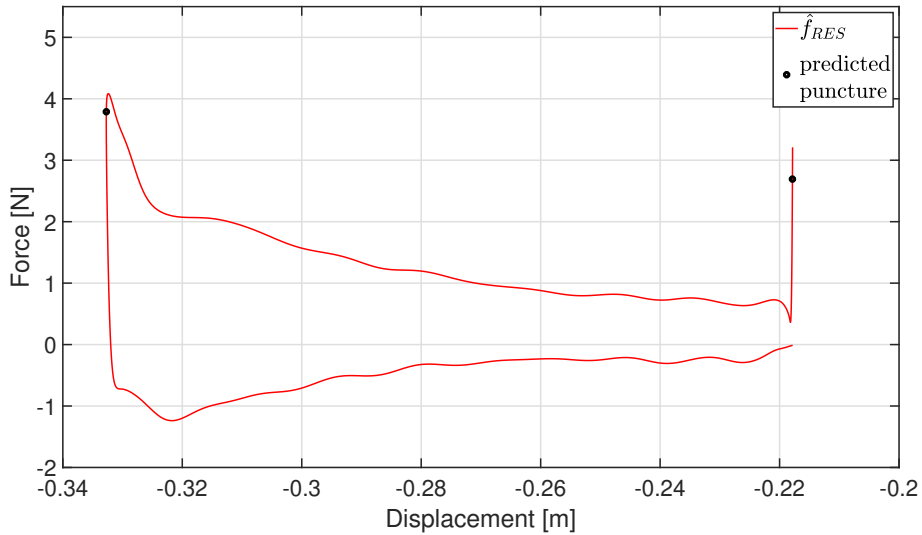


Figure 17: Evolution of the interaction force as a function of displacement. The black points represent the predicted layer transitions

Two layer ruptures are predicted from the algorithm, as seen in Figure 17. Anyway, the second rupture is probably a false positive. In fact, even if the needle is pushing on the underlying layer, the rupture does not occur (notice how the displacement does not increase even if the force decreases). This is caused by the inversion of motion of the needle: in fact, in Figure 19 it can be seen how the flag raises in correspondence with this event.

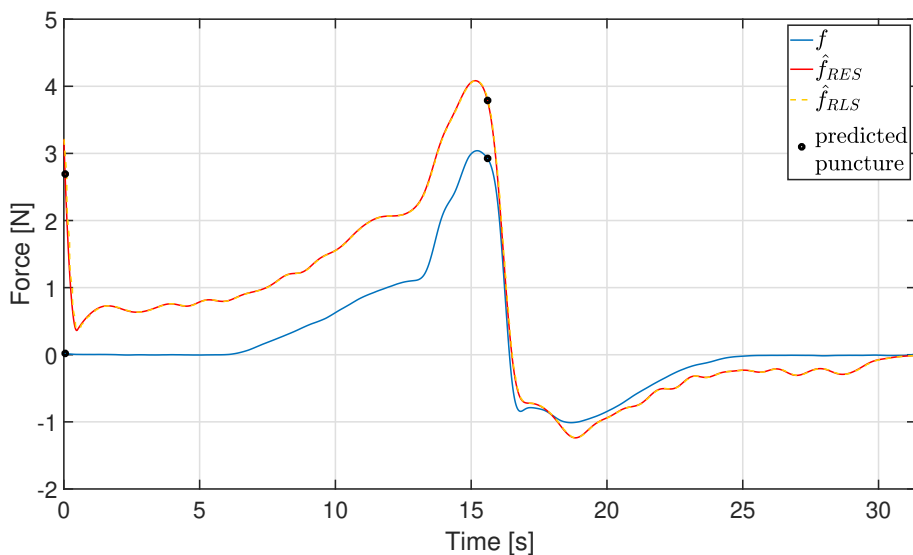


Figure 18: Evolution of the interaction force as a function of time. The black points represent the predicted layer transitions

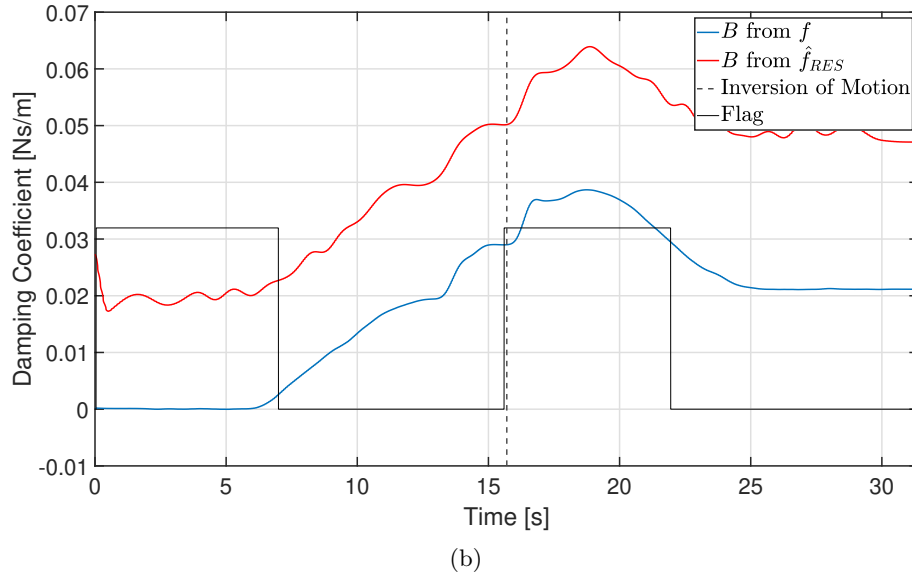
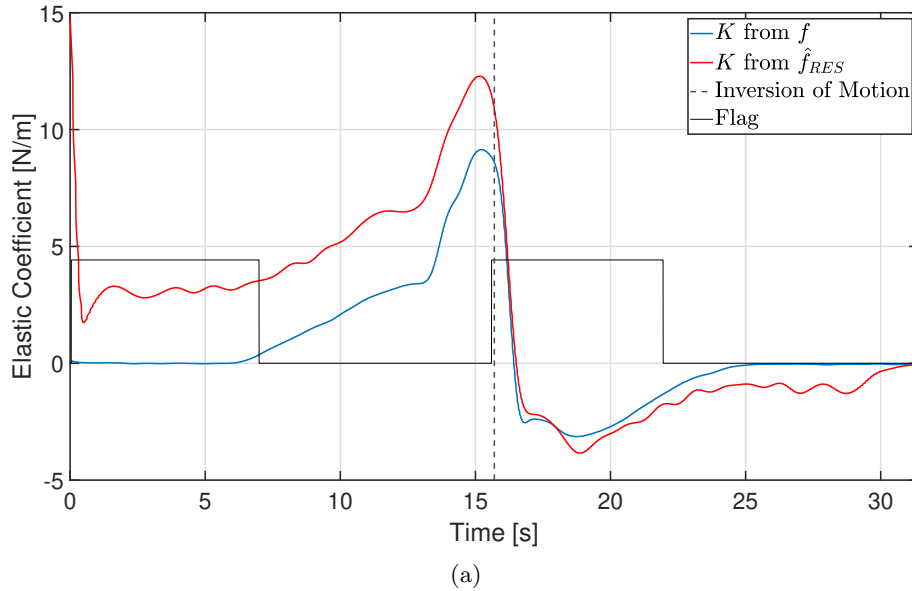
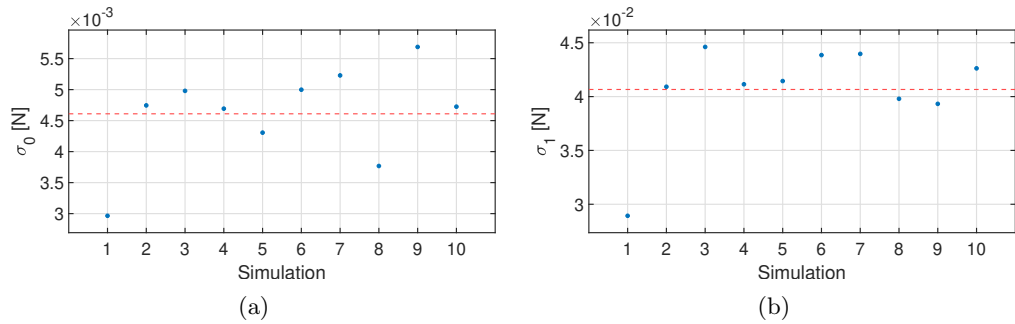


Figure 19: Predicted elastic (a) and damping (b) coefficients, with flag function. In blue, the coefficients obtained from the measured force; in red, the coefficients obtained from the residual force

Data from ten different simulations were available but we reported the results of one sinusoidal automatic trajectory, with the needle starting not in contact with the gel. The following plots show the values of σ_0 and σ_1 for all these simulations, together with their average.

Figure 20: Values of σ_0 (a) and σ_1 (b) for each experiment and their average (red)

Teleoperated Trajectory on Gel

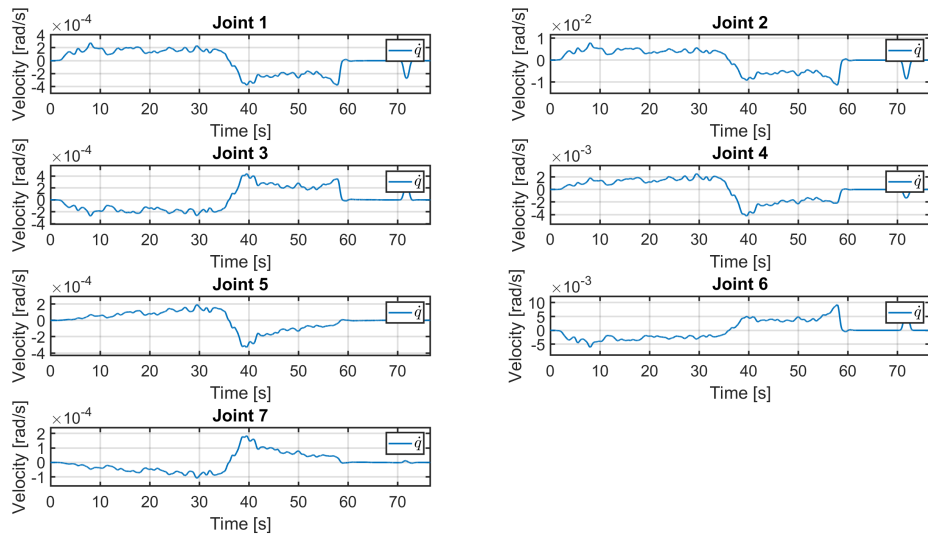


Figure 21: Joint velocities

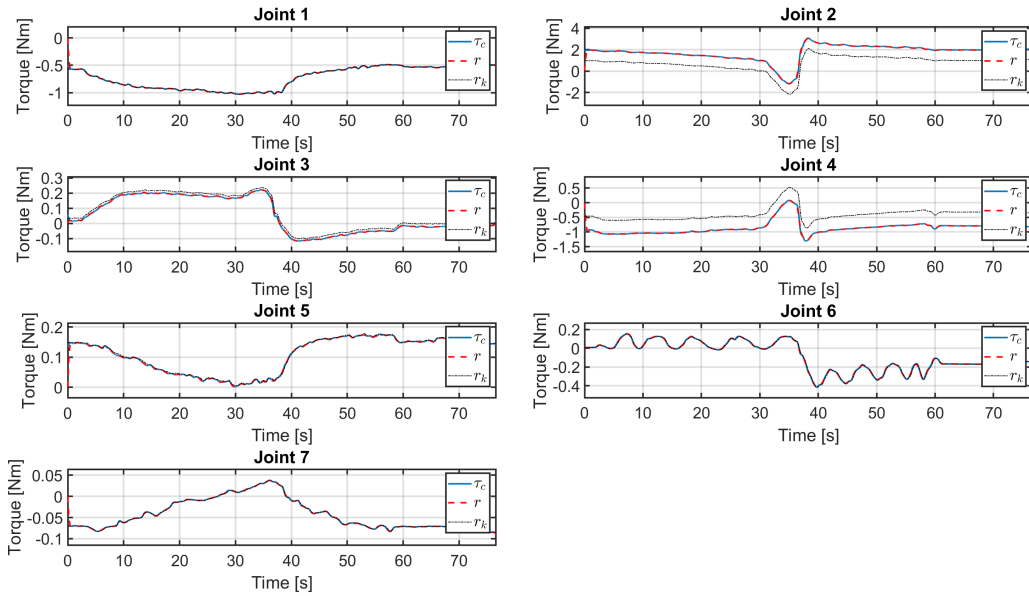


Figure 22: Disturbance joint torque (blue), residuals (red) and residuals retrieved from the Fast Research Interface of KUKA (black)

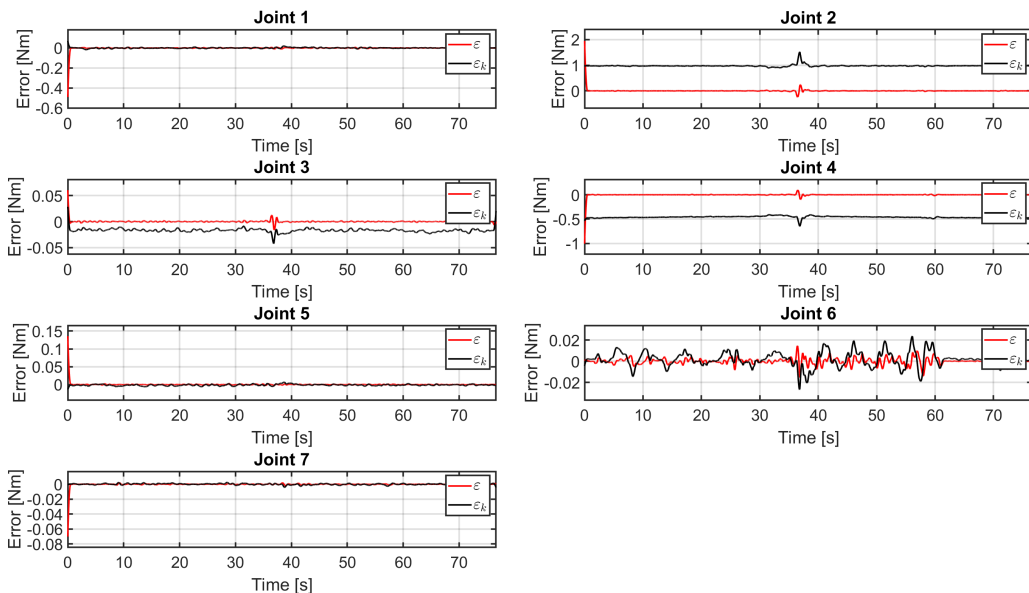


Figure 23: Reconstruction error of residuals (red) and residuals retrieved from the Fast Research Interface of KUKA (black)

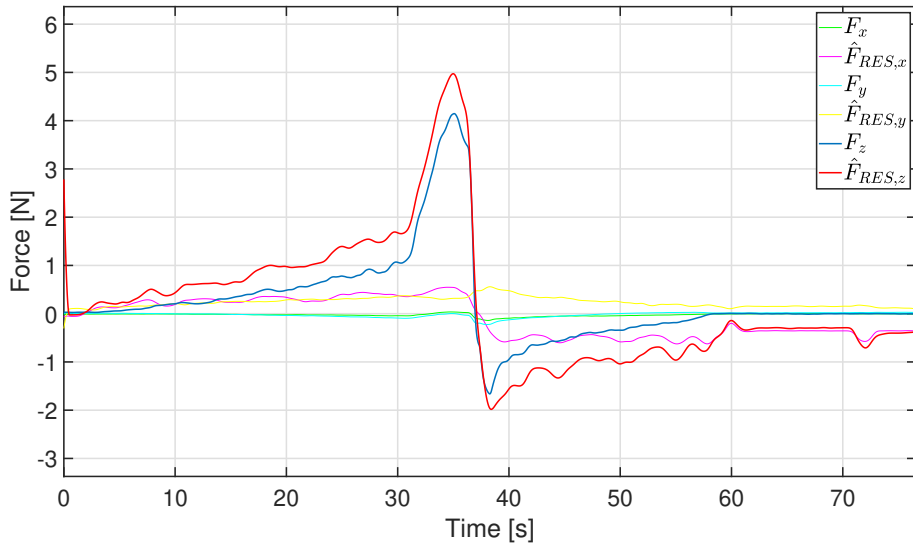


Figure 24: Measured force and reconstructed force from residuals. In particular, the components on the z -axis are in blue (measured) and red (residuals)

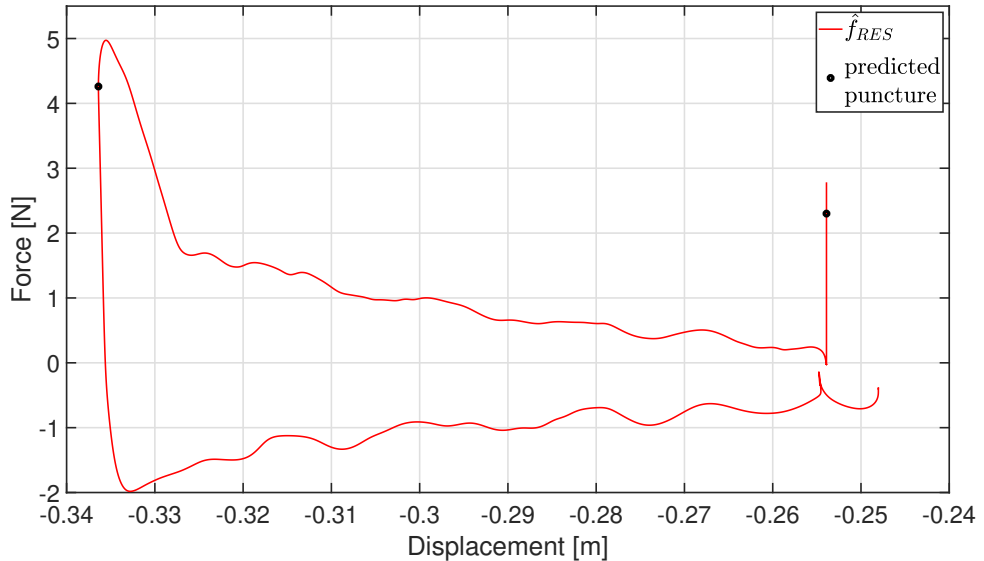


Figure 25: Evolution of the interaction force as a function of displacement. The black points represent the predicted layer transitions

Two layer ruptures are predicted from the algorithm, as seen in Figure 25. Anyway, the second rupture is probably a false positive. In fact, even if the needle is pushing on the underlying layer, the rupture does not occur (notice how the displacement does not increase even if the force decreases). This is caused by the inversion of motion of the needle.

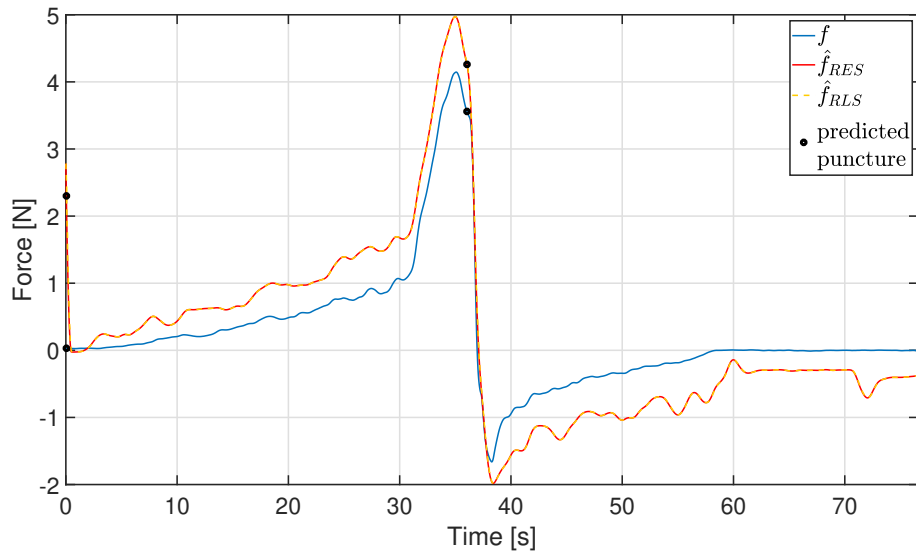
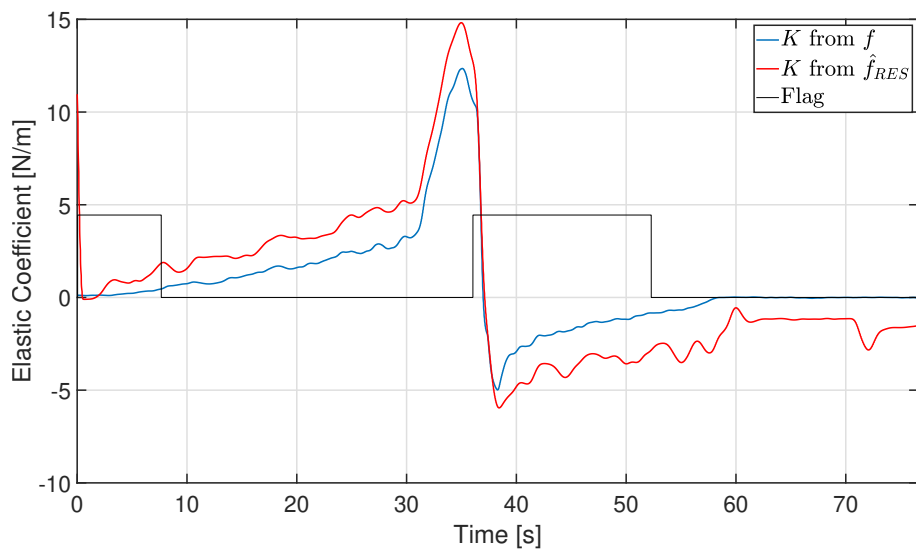


Figure 26: Evolution of the interaction force as a function of time. The black points represent the predicted layer transitions



(a)

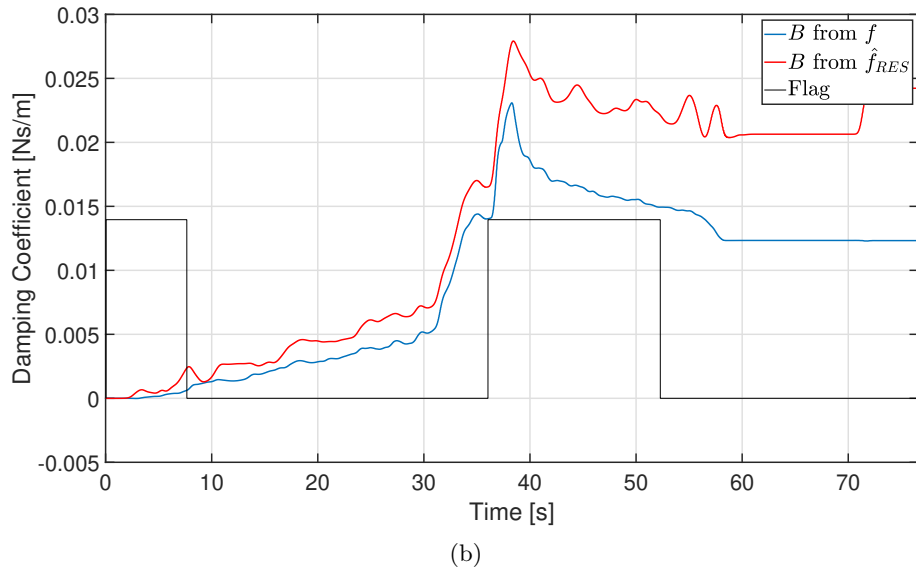


Figure 27: Predicted elastic (a) and damping (b) coefficients, with flag function. In blue, the coefficients obtained from the measured force; in red, the coefficients obtained from the residual force

Data from ten different simulations were available but we reported the results of one teleoperated trajectory, with the needle starting in contact with the gel. The following plots show the values of σ_0 and σ_1 for all these simulations, together with their average.

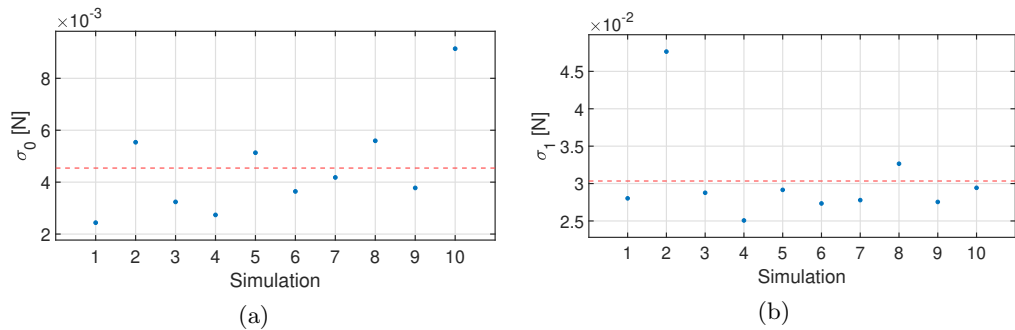


Figure 28: Values of σ_0 (a) and σ_1 (b) for each experiment and their average (red)

Sinusoidal Automatic Trajectory on Liver

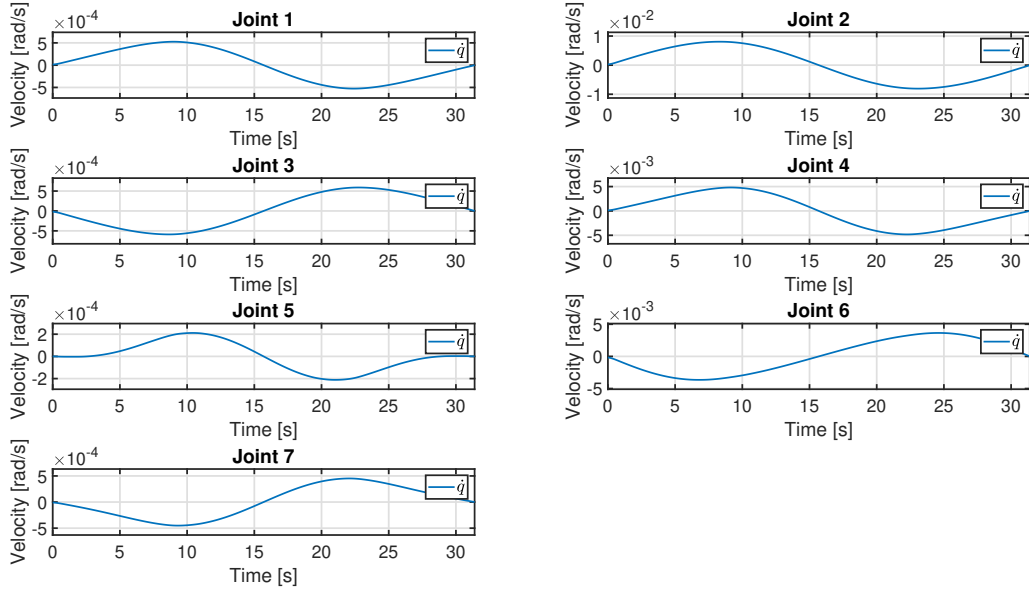


Figure 29: Joint velocities

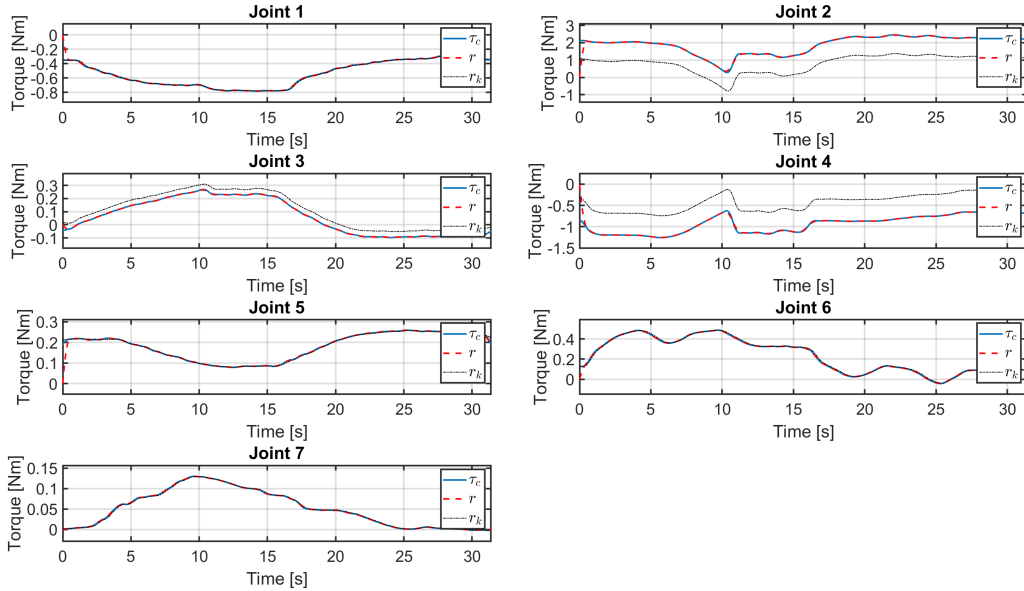


Figure 30: Disturbance joint torque (blue), residuals (red) and residuals retrieved from the Fast Research Interface of KUKA (black)

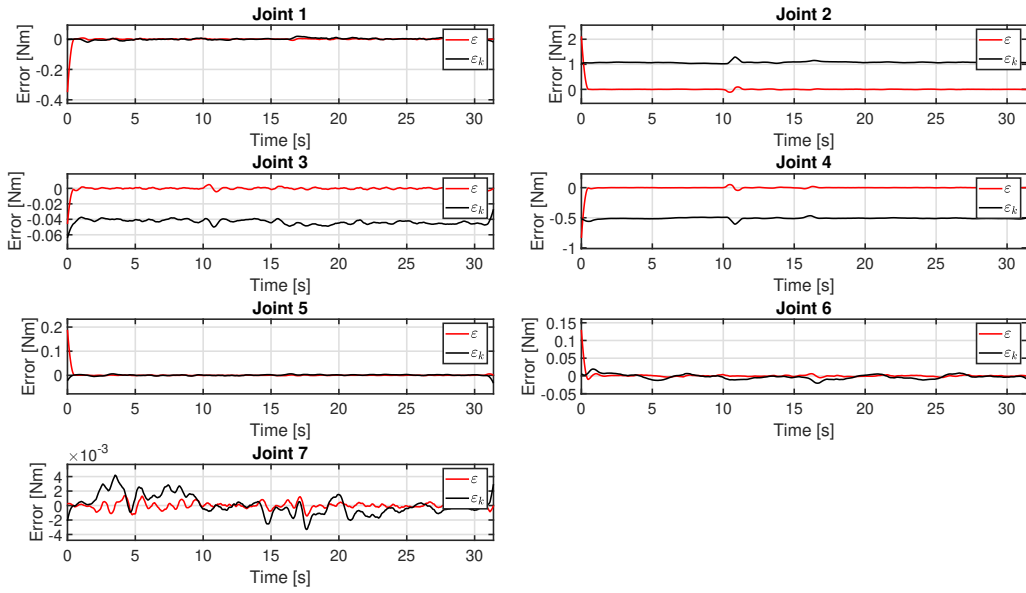


Figure 31: Reconstruction error of residuals (red) and residuals retrieved from the Fast Research Interface of KUKA (black)

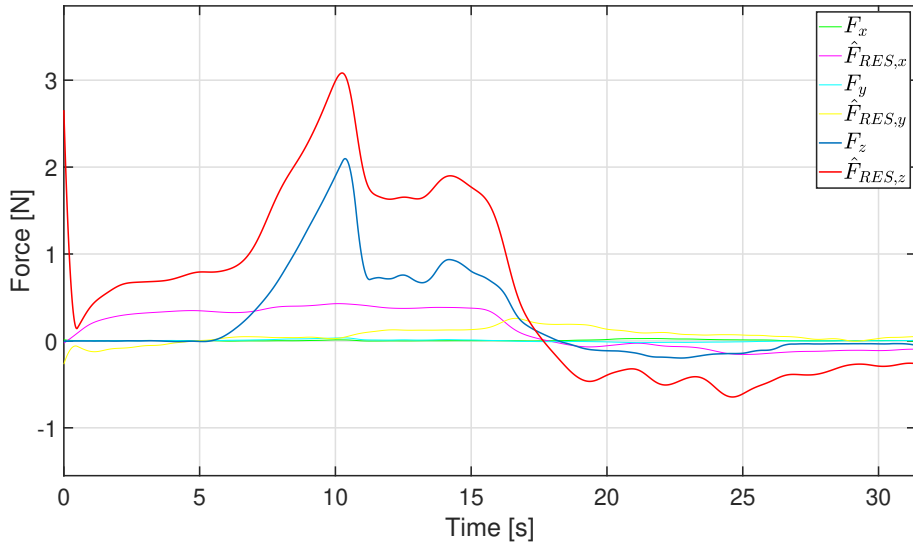


Figure 32: Measured force and reconstructed force from residuals. In particular, the components on the z -axis are in blue (measured) and red (residuals)

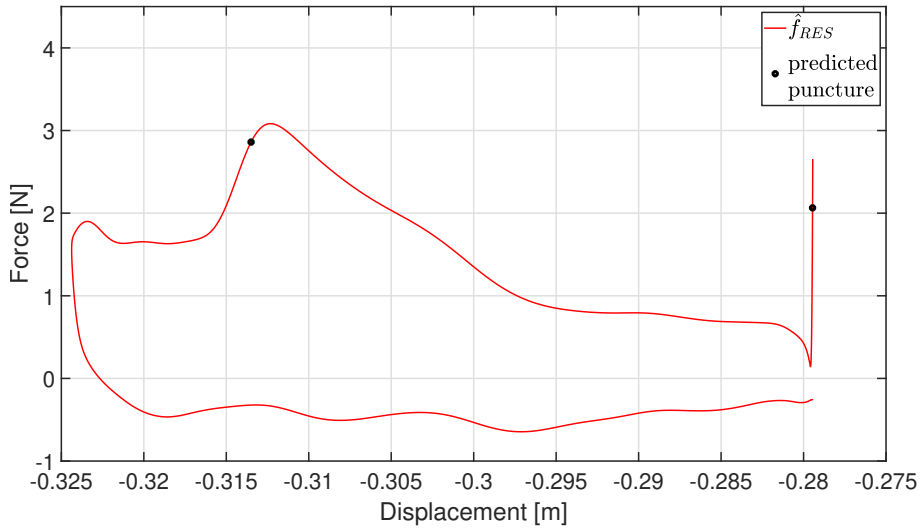


Figure 33: Evolution of the interaction force as a function of displacement. The black points represent the predicted layer transitions

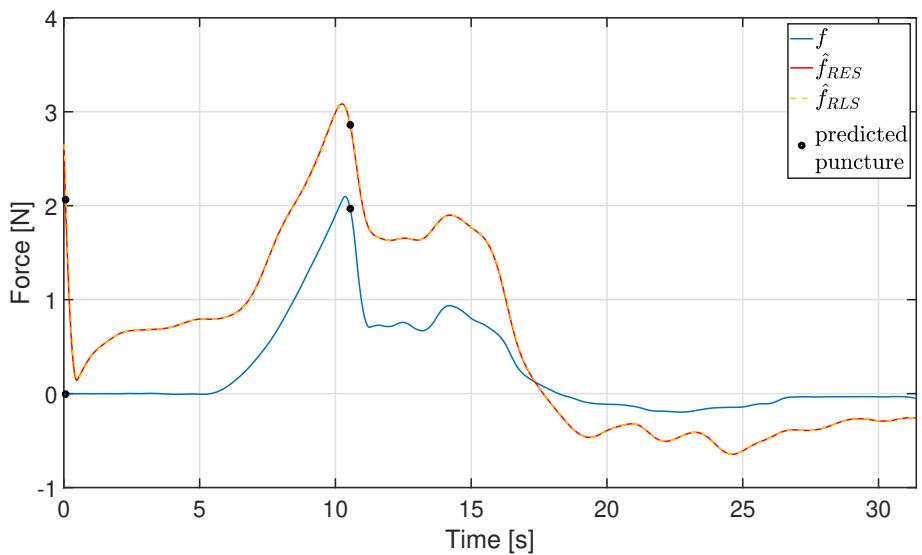


Figure 34: Evolution of the interaction force as a function of time. The black points represent the predicted layer transitions

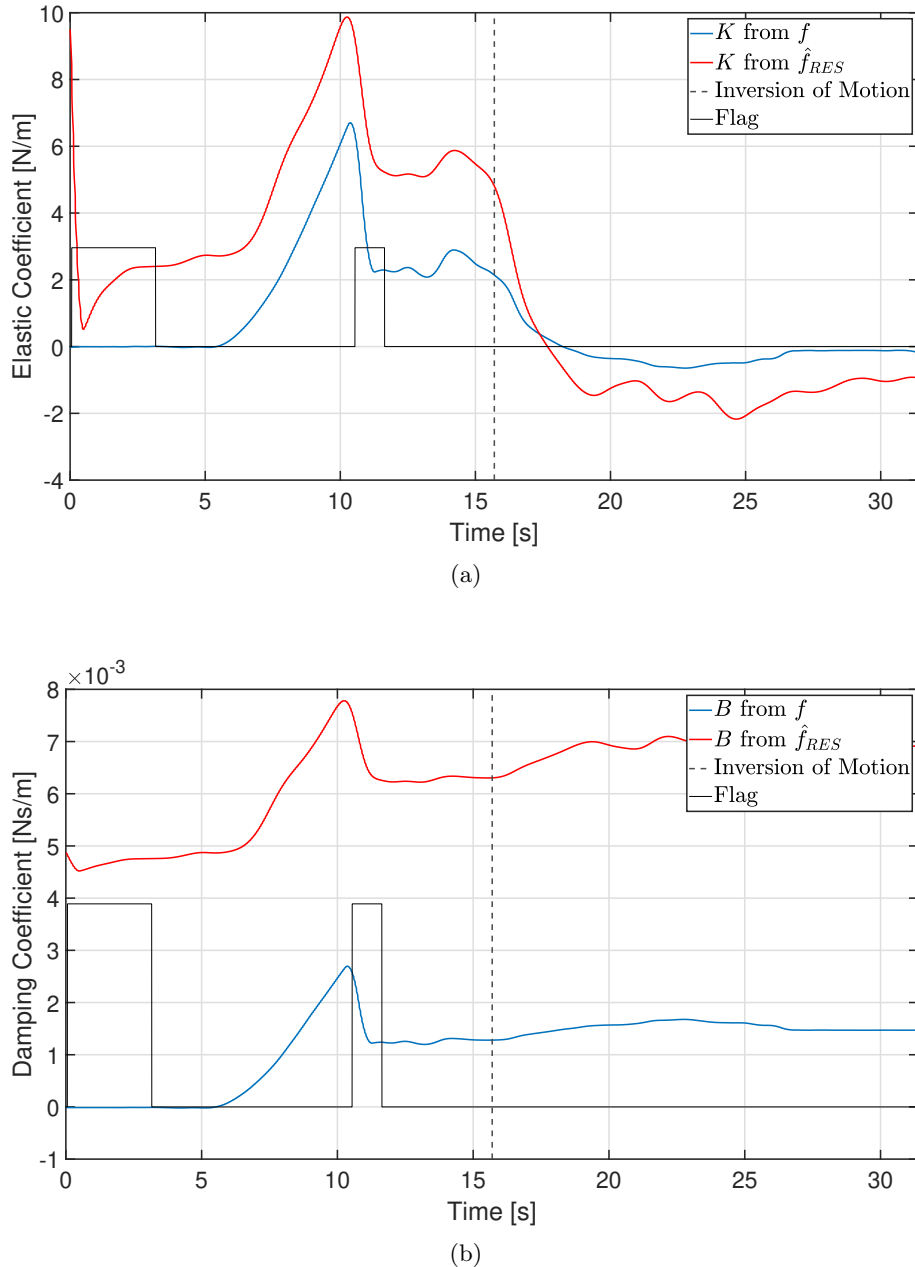


Figure 35: Predicted elastic (a) and damping (b) coefficients, with flag function. In blue, the coefficients obtained from the measured force; in red, the coefficients obtained from the residual force

Data from ten different simulations were available but we reported the results of one sinusoidal automatic trajectory, with the needle starting in contact with the liver. The following plots show the values of σ_0 and σ_1 for all these simulations, together with their average.

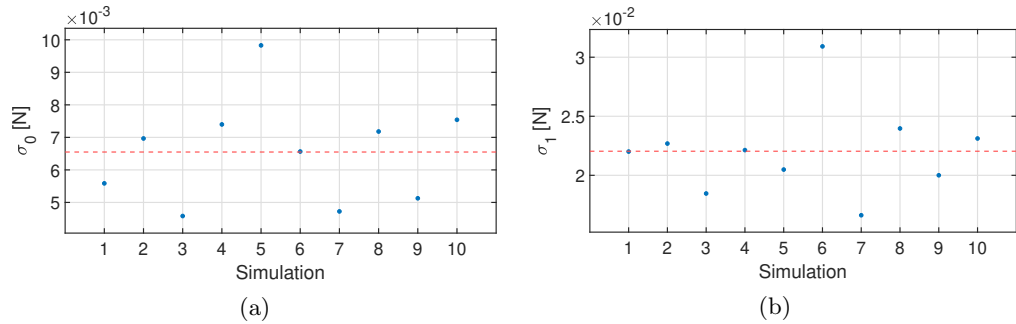


Figure 36: Values of σ_0 (a) and σ_1 (b) for each experiment and their average (red)

These data have been also processed using a dynamical model that takes into account also the presence of nonconservative forces. Denoting with τ_f the torque caused by joint friction (dependent on the joint velocity), equation (1) is replaced by

$$B(q) \ddot{q} + C(q, \dot{q}) \dot{q} + g(q) = \tau - \tau_f(\dot{q}) + J_c^T(q) F = \tau_{tot}. \quad (12)$$

Therefore, τ_f contributes in the residual equation (2) with a minus sign in the integral. It is interesting to notice how the results retrieved by the dynamical model in (12) are quite similar to the less accurate model in (1), as shown in the following pictures.

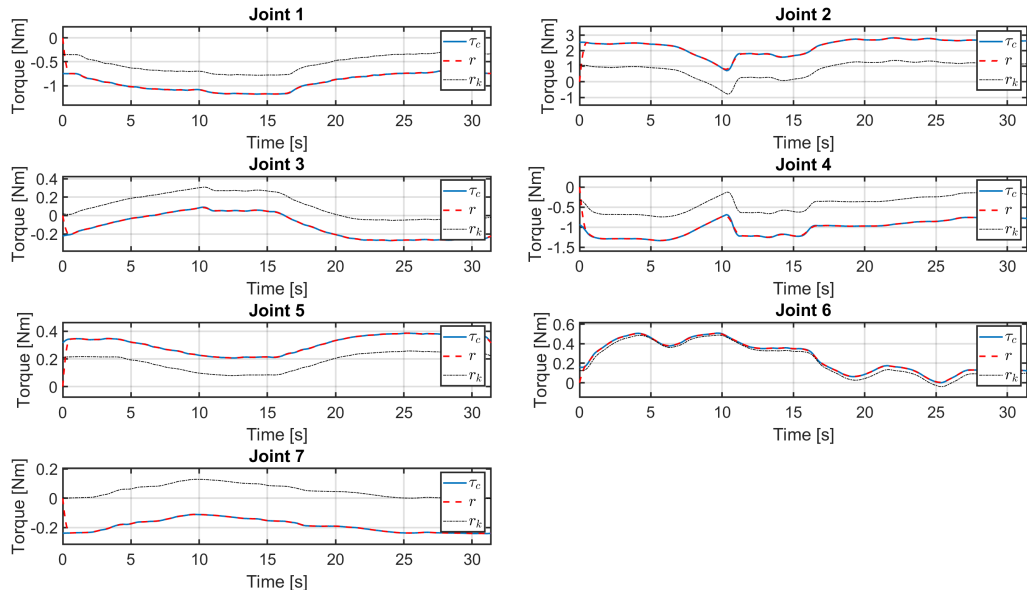


Figure 37: Disturbance joint torque (blue), residuals obtained using the model with joint friction (red) and residuals retrieved from the Fast Research Interface of KUKA (black)

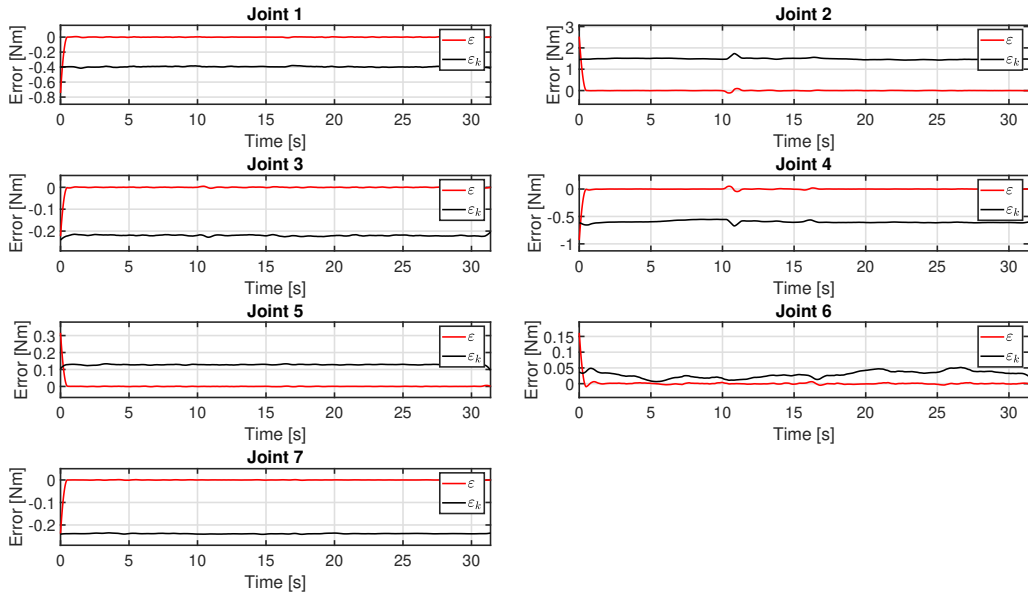


Figure 38: Reconstruction error of residuals obtained using the model with joint friction (red) and residuals retrieved from the Fast Research Interface of KUKA (black)

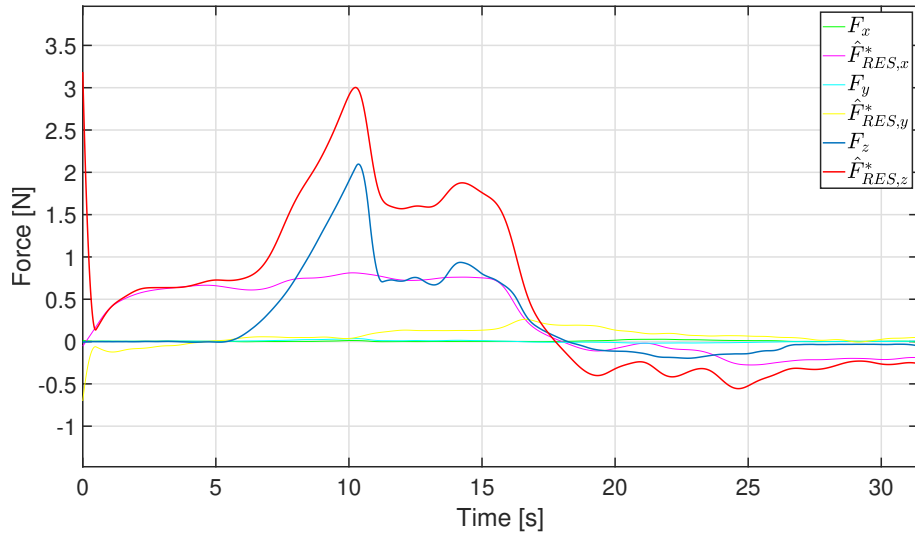


Figure 39: Measured force and reconstructed force from residuals obtained using the model with joint friction. In particular, the components on the z -axis are in blue (measured) and red (residuals)

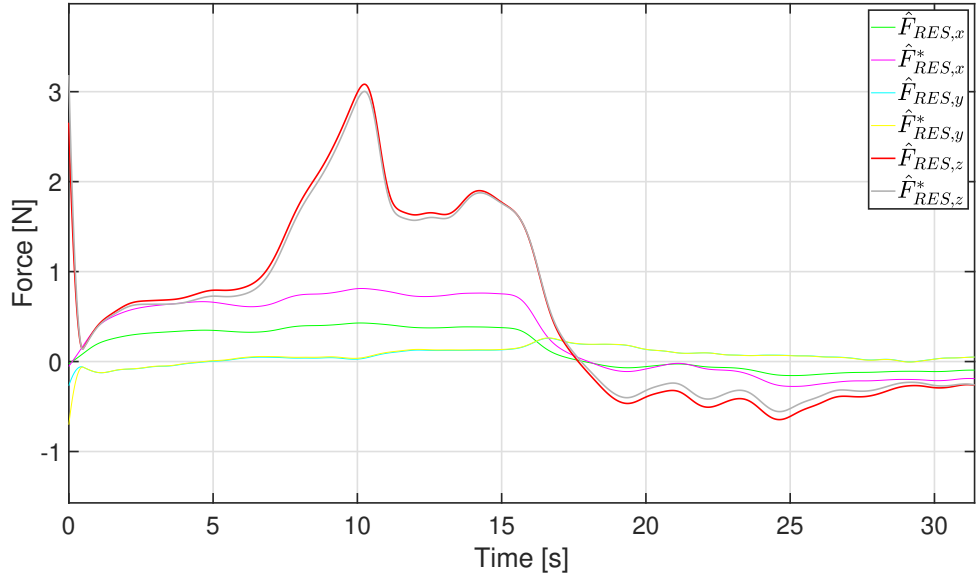


Figure 40: Components of the force reconstructed from residuals using the models in (1) and in (12). The symbol * denotes variables retrieved by the model with joint friction

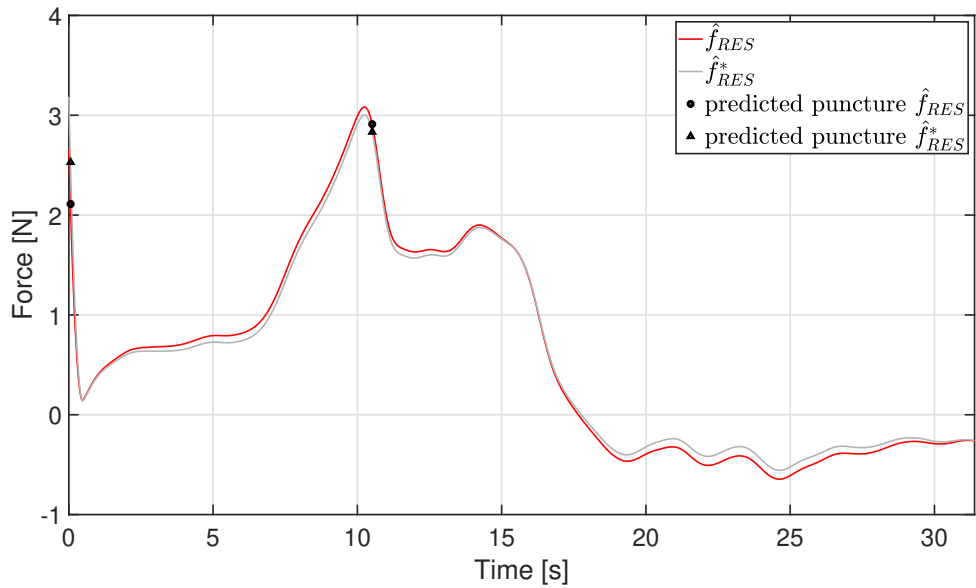


Figure 41: Evolution of the interaction force as a function of displacement. The black points represent the predicted layer transitions. The symbol * denotes variables retrieved by the model with joint friction

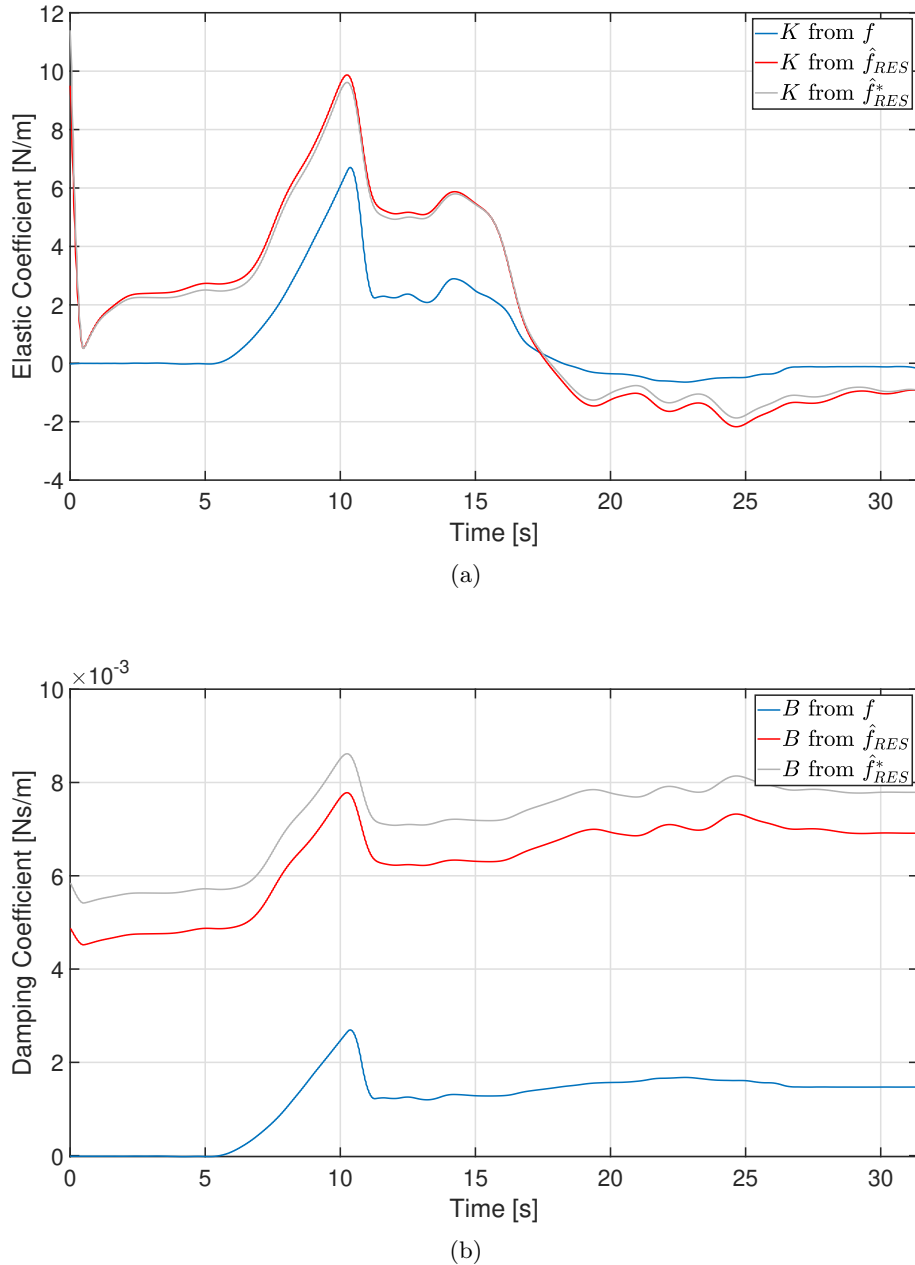


Figure 42: Predicted elastic (a) and damping (b) coefficients. In blue, the coefficients obtained from the measured force; in red, the coefficients obtained from the residual force using model (1); in grey, the coefficients obtained from the residual force using model (12). The symbol * denotes variables retrieved by the model with joint friction

Teleoperated Trajectory on Liver

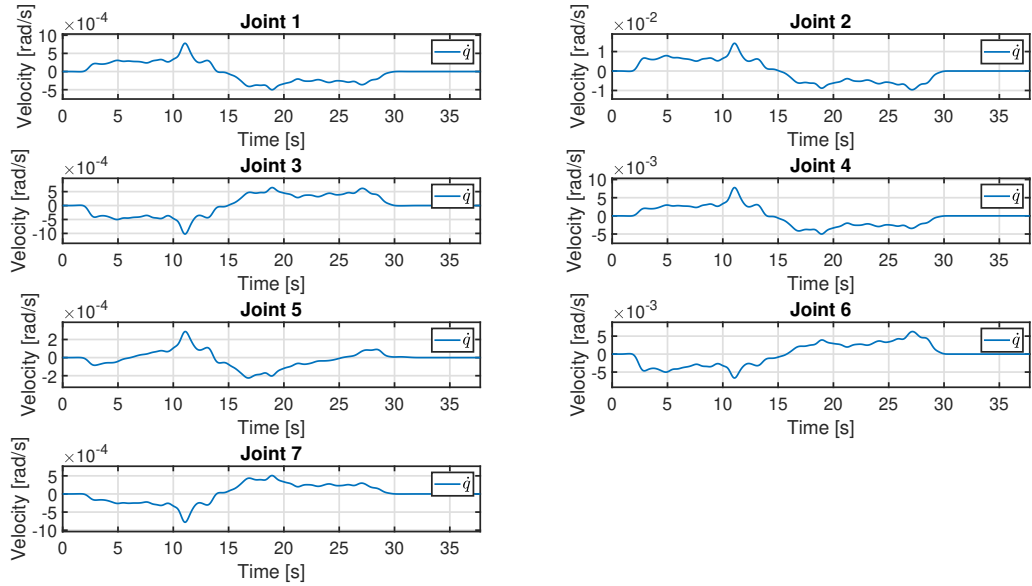


Figure 43: Joint velocities

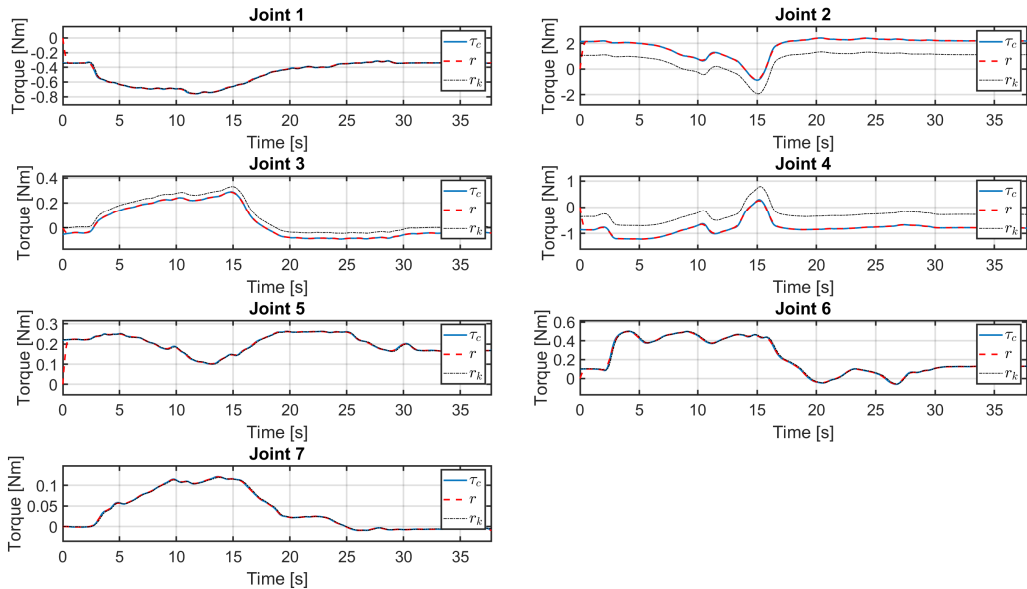


Figure 44: Disturbance joint torque (blue), residuals (red) and residuals retrieved from the Fast Research Interface of KUKA (black)

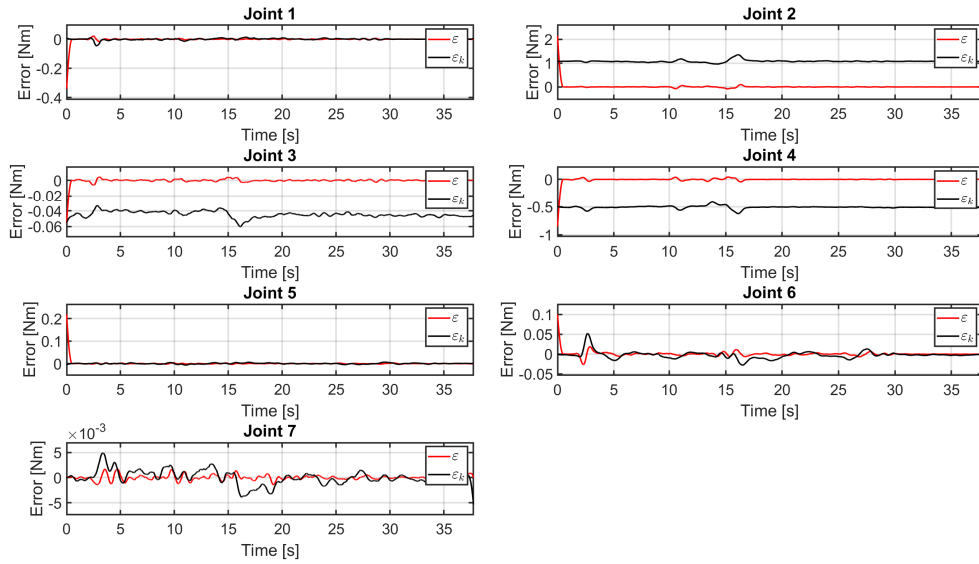


Figure 45: Reconstruction error of residuals (red) and residuals retrieved from the Fast Research Interface of KUKA (black)

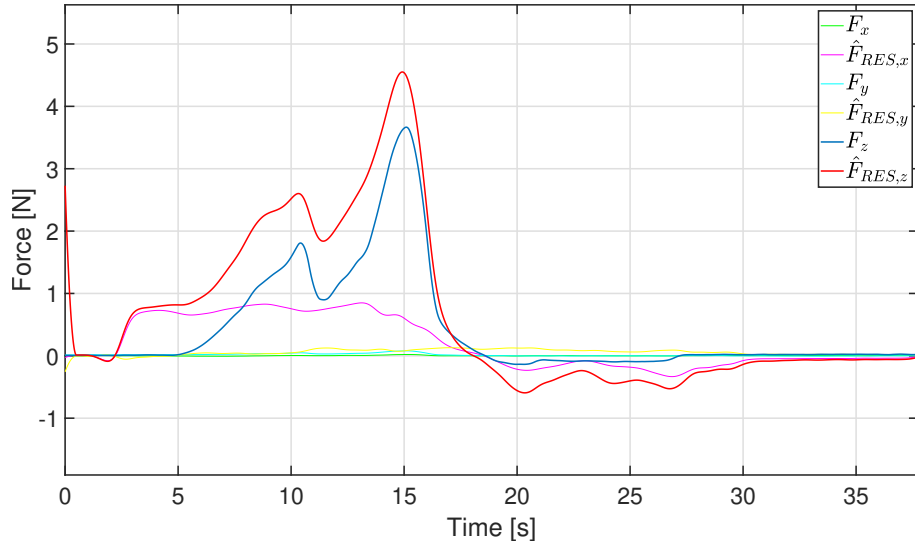


Figure 46: Measured force and reconstructed force from residuals. In particular, the components on the z -axis are in blue (measured) and red (residuals)

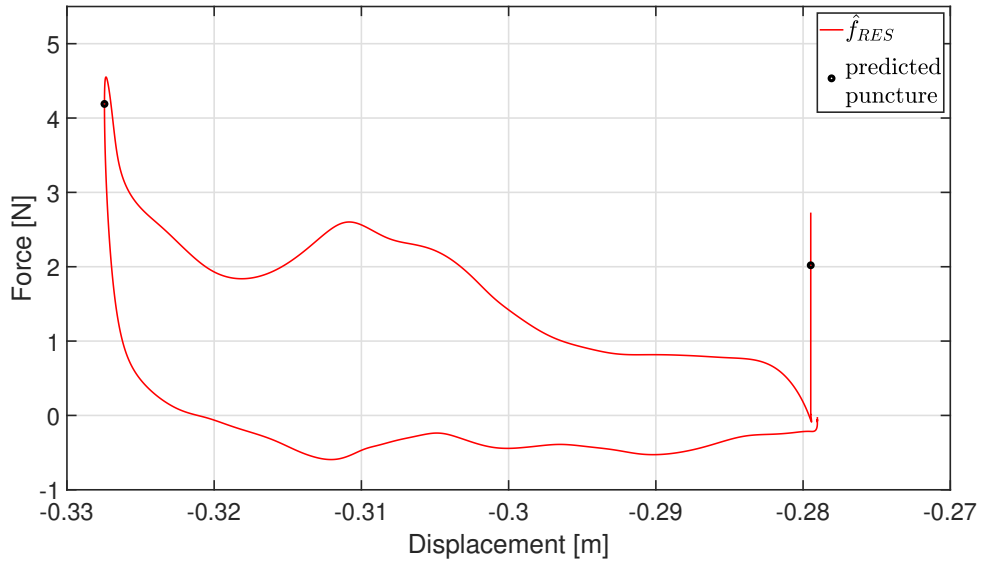


Figure 47: Evolution of the interaction force as a function of displacement. The black points represent the predicted layer transitions

Two layer ruptures are predicted from the algorithm, as seen in Figure 25. Anyway, the second rupture is probably a false positive. In fact, even if the needle is pushing on the underlying layer, the rupture does not occur (notice how the displacement does not increase even if the force decreases). This is caused by the inversion of motion of the needle.

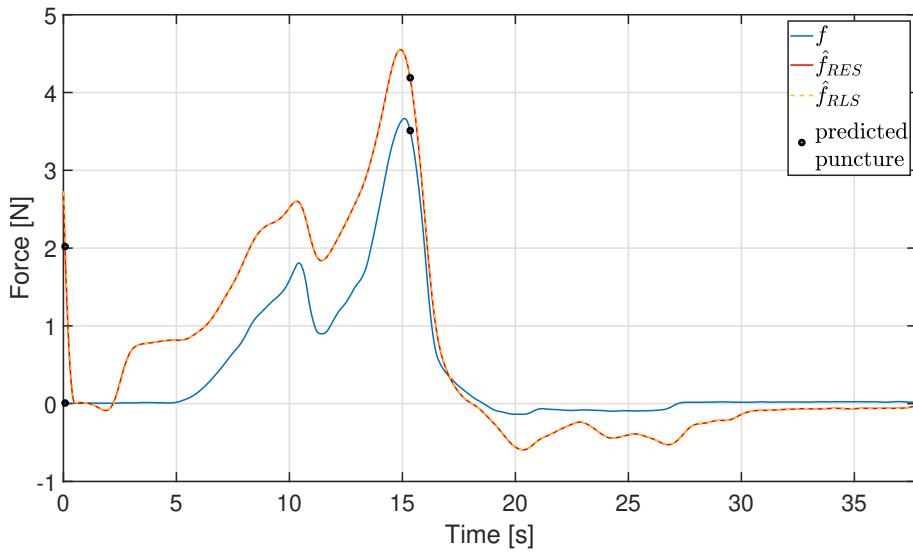


Figure 48: Evolution of the interaction force as a function of time. The black points represent the predicted layer transitions

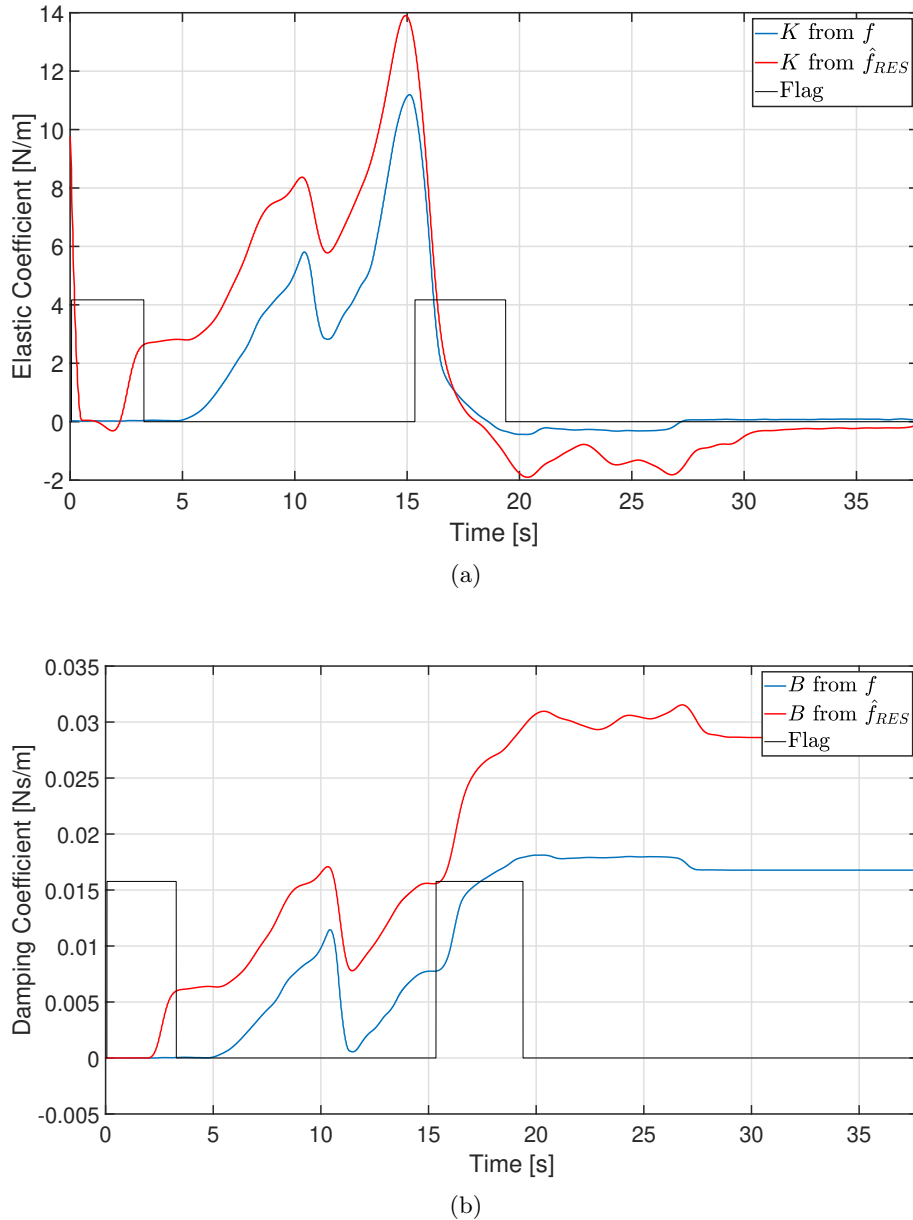


Figure 49: Predicted elastic (a) and damping (b) coefficients, with flag function. In blue, the coefficients obtained from the measured force; in red, the coefficients obtained from the residual force

Data from ten different simulations were available but we reported the results of one sinusoidal automatic trajectory, with the needle starting in contact with the liver. The following plots show the values of σ_0 and σ_1 for all these simulations, together with their average.

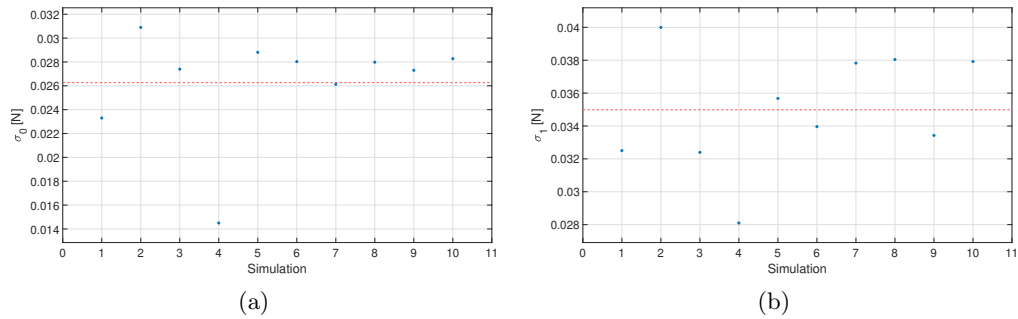


Figure 50: Values of σ_0 (a) and σ_1 (b) for each experiment and their average (red)

Conclusions

The needle insertion problem has been addressed. The contact of the needle with a tissue has been seen as a fault event; therefore, the residual method has been used for estimating the interaction force having only proprioceptive measurements. Then, the Recursive Least Squares algorithm has been applied for computing the visco-elastic parameters and for predicting rupture events. Finally, we showed the effectiveness of this procedure presenting the results on tissues of different nature.

References

- [1] Siciliano, B., Sciavicco, L., Villani, L., & Oriolo, G. (2010). "Robotics: modelling, planning and control". Springer Science & Business Media.
- [2] Evangelista, D., Iodice, F., Perica, A., Cefalo, M., Magrini, E., Anzidei, M., Vendittelli, M. (2016) "Residual-based interaction force estimation for haptic feedback in teleoperated needle insertion". *6th Joint Workshop on New Technologies for Computer/Robot Assisted Surgery (CRAS 2016)*.
- [3] Mattone, R., & De Luca, A. (2003). "Fault detection and isolation in robot manipulators". *IFATIS, IRAR002R01*.
- [4] De Luca, A., & Mattone, R. (2005). "Sensorless robot collision detection and hybrid force/motion control". In *Proceedings of the 2005 IEEE international conference on robotics and automation* (pp. 999-1004). IEEE.
- [5] Cacciotti, N., Cifonelli, A., Gaz, C., Paduano, V., Russo, A. V., Vendittelli, M. (2018). "Enhancing force feedback in teleoperated needle insertion through on-line identification of the needle-tissue interaction parameters". *IEEE RAS and EMBS International Conference on Biomedical Robotics and Biomechatronics (BIOROB)*.